arXiv:1107.3862v2 [cs.IT] 13 Sep 2011

Achieving "Massive MIMO" Spectral Efficiency with a Not-so-Large Number of Antennas

Hoon Huh, *Student Member, IEEE*,
Giuseppe Caire, *Fellow, IEEE*,
Haralabos C. Papadopoulos, *Member, IEEE*,
and Sean A. Ramprashad, *Senior Member, IEEE*

Index Terms

Channel training, downlink scheduling, frequency reuse, inter-cell cooperation, large-system analysis, linear precoding, Massive MIMO, pilot contamination, time-division duplex

H. Huh and G. Caire are with the Department of Electrical Engineering, University of Southern California, Los Angeles, CA 90089, USA. (e-mail: {hhuh, caire}@usc.edu)

H. C. Papadopoulos and S. A. Ramprashad are with DOCOMO USA Labs, Palo Alto, CA 94304, USA. (e-mail: {hpapadopoulos, ramprashad}@docomolabs-usa.com)

Abstract

Time-Division Duplexing (TDD) allows to estimate the downlink channels for an arbitrarily large number of base station antennas from a finite number of orthogonal pilot signals in the uplink, by exploiting channel reciprocity. Therefore, while the number of users per cell served in any time-frequency channel coherence block is necessarily limited by the number of pilot sequence dimensions available, the number of base station antennas can be made as large as desired. Based on this observation, a recently proposed very simple "Massive MIMO" scheme was shown to achieve unprecedented spectral efficiency in realistic conditions of user spatial distribution, distance-dependent pathloss and channel coherence time and bandwidth.

The main focus and contribution of this paper is a novel network-MIMO TDD architecture that achieves spectral efficiencies comparable with "Massive MIMO", with one order of magnitude fewer antennas per active user per cell. The proposed architecture is based on a family of network-MIMO schemes defined by small clusters of cooperating base stations, zero-forcing multiuser MIMO precoding with suitable inter-cluster interference constraints, uplink pilot signals reuse across cells, and frequency reuse. The key idea consists of partitioning the users population into geographically determined "bins", such that all users in the same bin are statistically equivalent, and use the optimal network-MIMO architecture in the family for each bin. A scheduler takes care of serving the different bins on the time-frequency slots, in order to maximize a desired network utility function that captures some desired notion of fairness. This results in a mixed-mode network-MIMO architecture, where different schemes, each of which is optimized for the served user bin, are multiplexed in time-frequency.

In order to carry out the performance analysis and the optimization of the proposed architecture in a clean and computationally efficient way, we consider the large-system regime where the number of users, the number of antennas, and the channel coherence block length go to infinity with fixed ratios. The performance predicted by the large-system asymptotic analysis matches very well the finite-dimensional simulations. Overall, the system spectral efficiency obtained by the proposed architecture is similar to that achieved by "Massive MIMO", with a 10-fold reduction in the number of antennas at the base stations (roughly, from 500 to 50 antennas).

I. INTRODUCTION

Multiuser MIMO (MU-MIMO) technology is being intensively studied for the next generation wireless cellular systems (e.g., LTE-Advanced [1]). Schemes where antennas of different Base Stations (BSs) are jointly processed by centralized BS controllers are usually referred to as "network-MIMO" architectures (e.g., [2]–[8]). It is well-known that the improvement obtained from transmit antenna joint processing is limited by a "dimensionality" bottleneck [9]–[11]. In particular, the high-SNR capacity of a single-user MIMO system with N_t transmit antennas, N_r receiving antennas, and fading coherence block length T complex dimensions,[1] scales as $C(\mathsf{SNR}) = \min\{N_t, N_r, T/2\} \log \mathsf{SNR} + O(1)$ [13], [14]. Therefore, even by pooling all base stations into a single distributed macro-transmitter with $N_t \gg 1$ antennas and all user terminals into a single distributed macro-receiver with $N_r \gg 1$ antennas, the system *degrees of freedom*[2] are eventually limited by the fading coherence block length T. While this dimensionality bottleneck is an inherent fact, emerging from the high-SNR behavior of the capacity of MIMO block-fading channels, [14] (see also [15]) the *same behavior* also characterizes the capacity scaling of MU-MIMO systems based on explicit training for channel estimation, and can be interpreted as the effect of the "overhead" incurred by pilot signals [16].

For frequency-division duplex (FDD) systems, the training overhead required to collect channel state information at the transmitters (CSIT) grows linearly with the number of cooperating transmit antennas. Such overhead restricts the MU-MIMO benefits that can be harvested with a large number of transmit antennas, as shown in [10] using system-level simulation and in [11] using closed-form analysis based on the limiting distribution of certain large random matrices.

For Time Division Duplexing (TDD) systems, exploiting *channel reciprocity* [17], [18], the CSIT can be obtained from the uplink training. In this case, the pilot signal overhead scales linearly with the number of *active users* per cell, but it is independent of the number of cooperating antennas at the BSs. As a result, for a fixed number of users scheduled for transmission, the TDD system performance can be significantly improved by increasing the number of BS antennas.

Following this idea, Marzetta [18] has shown that simple *Linear Single-User BeamForming* (LSUBF)

[1]The fading coherence block length T, measured in signal complex "dimensions" in the time-frequency domain is proportional to the product $W_c T_c$, where T_c (s) denotes the channel coherence interval, and W_c (Hz) denotes the channel coherence bandwidth [12].

[2]The system Degrees of Freedom (DoFs) are defined as the pre-log factor of the system capacity $C(\mathsf{SNR})$, i.e., $\mathrm{DoFs} = \lim_{\mathsf{SNR}\to\infty} \frac{C(\mathsf{SNR})}{\log \mathsf{SNR}}$, and quantify the number of "equivalent" parallel single-user Gaussian channels, in a first-order approximation with respect to $\log \mathsf{SNR}$.

and random user scheduling, without any inter-cell cooperation, yields unprecedented spectral efficiency in TDD cellular systems, provided that a *sufficiently* large number of transmit antennas per active user are employed at each BS. This scheme, nicknamed hereafter "Massive MIMO", was analyzed in the limit of infinite number of BS antennas per user per cell. In this regime, the effects of Gaussian noise and uncorrelated inter-cell interference disappear, and that the only remaining impairment is the inter-cell interference due to *pilot contamination* [19], i.e., to the correlated interference from other cells due to users re-using the same pilot signal (see Section III).

In this work, we also focus on TDD systems and exploit reciprocity. The main contribution of this paper is a novel network-MIMO architecture that achieves spectral efficiencies comparable with "Massive MIMO", with a more practical number of BS antennas per active user (one order of magnitude less antennas for approximately the same spectral efficiency). As in [18], we also analyze the proposed system in the limit of a large number of antennas. However, a different system scaling is considered, where the number of antennas per active user per cell is *finite*. This is obtained by letting the number of users per cell, the number of antennas per BS, and the channel coherence block length go to infinity, with fixed ratios [11]. We find that in this regime the LSUBF scheme advocated in [18] performs very poorly. In contrast, we consider a family of network-MIMO schemes based on small clusters of cooperating base stations, *Linear Zero-Forcing BeamForming* (LZFBF) with suitable inter-cluster interference constraints, uplink pilot signals reuse across cells, and frequency reuse. The key idea consists of partitioning the users population into geographically determined "bins", containing statistically equivalent users, and optimizing the network-MIMO scheme for each individual bin. Then, users in different bins are scheduled over the time-frequency slots, in order to maximize an appropriately chosen network utility function reflecting some desired notion of "fairness". The geographic nature of the proposed scheme yields very simple system operations, where each time a given bin is scheduled, a subset of *active users* in the selected bin is chosen at random or in a deterministic round robin fashion, without performing any CSIT-based user selection. This allows a fast turn-around between feedback and transmission, that can take place in the same channel coherence block. The resulting architecture is a mixed-mode network-MIMO, where different schemes, each of which is optimized for the served user bin, are multiplexed in time-frequency.

Using results and tools from the large-system analysis developed in [11], [20] and adapted to the present scenario, we obtain the asymptotic achievable rate for each scheme in closed form. The performance predicted by the large-system analysis match very well with finite-dimensional simulations, in agreement with [11], [21] and with several well-known works on single-user MIMO in the large antenna regime [22], [23]. The large-system analysis developed here is instrumental to the systematic design and optimization

of the proposed system architecture, since it allows an accurate and rapid selection of the best network-MIMO scheme for each user bin without resorting to cumbersome and time-consuming Monte Carlo simulation. In fact, the system parameters in the considered family of network-MIMO schemes are strongly mutually dependent, and the system optimization without the analytical tools developed here would just be infeasible.

We hasten to say that the ideas of dynamic clustering of cooperating BSs, and multimodal MU-MIMO downlink have appeared in a large number of previous works (see for example [24]–[28]. Giving a fair account of this vast literature would be impossible within the space limits of this paper. Nevertheless, we wish to stress here that the novel contribution of this paper is a *systematic approach* to multi-modal system optimization based on simple closed-form expressions of the spectral efficiency of each network-MIMO scheme in the family, and on scheduling across the schemes (or "modes") in order to maximize a desired network utility function.

The remainder of this paper is organized as follows. In Section II, we describe the family of proposed network-MIMO schemes. We discuss the uplink training, MMSE channel estimation and pilot contamination effect for TDD-based systems in Section III. In Section IV, we analyze the network-MIMO architectures under considerations and and provide expressions for their achievable rate in the large-system limit. Scheduling under specific fairness criteria and the corresponding system spectral efficiency is presented in Section V. Numerical results including comparison with finite dimensional simulation results are presented in Section VI and concluding remarks are given in Section VII.

II. System model

The TDD cellular architecture for high-data rate downlink proposed in this work is based on the following elements:

1) A family of network-MIMO schemes, defined in terms of the size and shape of clusters of cooperating BSs, pilot reuse across clusters, frequency reuse factor, and downlink linear precoding scheme;
2) A partitioning of the user population into bins, according to their position in the cellular coverage area;
3) The determination of the optimal network-MIMO scheme in the family for each user bin, creating an association between user bins and network-MIMO schemes;
4) Scheduling of the user bins in time-frequency in order to maximize a suitable concave and componentwise non-decreasing network utility function of the ergodic user rates. The network utility

function is chosen in order to reflect some desired notion of fairness (e.g., proportional fairness [21], [29]–[32]). When a given bin is scheduled, the associated optimized network-MIMO architecture is used.

Invoking well-known convergence results [22], [23], we use the "large-system analysis" approach for multi-antenna cellular systems pioneered in [21], [33]–[35]. In particular, we use the results of [11], which can be easily applied to our system model, and analyze the performance of the network-MIMO schemes in the considered family while scaling the number of users in each bin, the number of antennas per BS and the small-scale fading coherence block length to infinity, with fixed ratios. We define a *system size* parameter indicated by N, and let all the above quantities scale linearly with $N \to \infty$. Specifically, we let MN denote the number of BS antennas, LN denote the channel coherence block length, and UN denote the number of users per location (a bin is defined as a set of discrete locations in the cellular coverage, see Section II-A), for given constants M, L and U.

A. Cellular layout and frequency reuse

Base stations, cells and clusters: The system geometry is concisely described by using lattices on the real line $\mathbb{R}$ (for 1-dimensional layouts [8], [10]) or on the real plane $\mathbb{R}^2$ (for 2-dimensional layouts [18]). Consider nested lattices $\Lambda \subseteq \Lambda_{\rm bs} \subseteq \Lambda_{\rm u}$ in $\mathbb{R}$ (resp., $\mathbb{R}^2$). The system *coverage region* is given by the Voronoi cell $\mathcal{V}$ of Λ centered at the origin.[3] BSs are located at points $b \in \Lambda_{\rm bs} \cap \mathcal{V}$. The finer lattice $\Lambda_{\rm u}$ defines a grid of discrete *user locations*, as explained later in this section. We let $B = |\Lambda_{\rm bs} \cap \mathcal{V}|$ denote the number of BSs in the system.

Example 1: Consider the 1-dimensional layout defined by $\Lambda = B\mathbb{Z}$ and $\Lambda_{\rm bs} = \mathbb{Z}$. The coverage region is $\mathcal{V} = [-B/2, B/2)$ and the BS locations b are given by all integer-coordinate points in the interval $[-B/2, B/2)$. $\lozenge$

Example 2: In system studies reported in the standardization of 4th generation cellular systems [36], [37] it is customary to consider a 2-dimensional hexagonal layout formed by 19 cells, as shown in Fig. 1. In this case, $\Lambda_{\rm bs} = \mathbf{A}\mathbb{Z}^2$ and $\Lambda = \mathbf{AB}\mathbb{Z}^2$, with

$$\mathbf{A} = \frac{\sqrt{3}r}{2}\begin{bmatrix}\sqrt{3} & 0\\ 1 & 2\end{bmatrix} \text{ and } \mathbf{B} = \begin{bmatrix}4 & \sqrt{3}\\ -\sqrt{3} & 4\end{bmatrix},$$

where r denotes the distance between the center of a small hexagon and one of its vertices. We have $B = \det(\mathbf{B}) = 19$, and the distance between the closest two points in $\Lambda_{\rm bs}$ is $\sqrt{3}r$. $\lozenge$

[3]The Voronoi cell of a lattice point $x \in \Lambda \in \mathbb{R}^n$ is the set of points $y \in \mathbb{R}^n$ closer to x than to any other lattice point.

For the sake of symmetry, in order to avoid "border effects" at the edges of the coverage region, all distances and all spatial coordinates are defined modulo Λ. The modulo Λ distance between two points u, v in $\mathbb{R}$ (resp., $\mathbb{R}^2$) is defined as

$$d_\Lambda(u,v) = |u - v \mod \Lambda|, \tag{1}$$

where $x \bmod \Lambda = x - \arg\min_{\lambda\in\Lambda} |x-\lambda|$. Cell $\mathcal{V}_b$ is defined as the Voronoi region of BS $b \in \Lambda_{\rm bs} \cap \mathcal{V}$ with respect to the modulo-Λ distance, i.e., $\mathcal{V}_b = \{x \in \mathbb{R} : d_\Lambda(x,b) \le d_\Lambda(x,b'), \ \ \forall\, b' \in \Lambda_{\rm bs} \cap \mathcal{V}\}$ (replace $\mathbb{R}$ with $\mathbb{R}^2$ for the 2-dimensional case). The collection of cells $\{\mathcal{V}_b\}$ forms a partition of $\mathcal{V}$ into congruent regions.

A "clustering pattern" $u(\mathcal{C})$, defined by the set of BS locations $\mathcal{C} = \{b_0, \ldots, b_{C-1}\}$ with $b_j \in \Lambda_{\rm bs} \cap \mathcal{V}$ and rooted at $b_0 = 0$, is the collection of BS location sets (referred to as "clusters" in the following)

$$u(\mathcal{C}) = \{\{\mathcal{C} + c\} \ : \ c \in \Lambda_{\rm bs} \cap \mathcal{V}\}. \tag{2}$$

We focus on systems based on single-cell processing ($C = 1$), or with joint processing over clusters of small size: $C = 2$ in the 1-dimensional case, and size $C = 3$ in the 2-dimensional case, as shown in Fig. 2. It turns out that larger clusters do not achieve better performance due to the large training overhead incurred, while requiring higher complexity. Therefore, our results are not restrictive in terms of cluster size, since they capture the best system parameters configurations.

Example 3: In the 1-dimensional case of Example 1, with $C = 1$ and $C = 2$, we have

$$u(\{0\}) = \{\{0\}, \{1\}, \ldots, \{B-1\}\}.$$

and

$$u(\{0,1\}) = \{\{0,1\}, \{1,2\}, \ldots, \{B-1, 0\}\},$$

respectively. $\lozenge$

User location bins: We assume a uniform user spatial distribution over the coverage region. For the sake of analytical simplicity, we discretize the user distribution into a regular grid of user locations, corresponding to the points of the lattice translate $\widetilde{\Lambda}_{\rm u} = \Lambda_{\rm u} + u_0$, where $u_0 \neq 0$ is chosen such that $\widetilde{\Lambda}_{\rm u}$ is symmetric with respect to the origin and no points of $\widetilde{\Lambda}_{\rm u}$ fall on the cell boundaries.

Example 4: In the 1-dimensional case of Example 1 we can choose $\Lambda_{\rm u} = \frac{1}{K}\mathbb{Z}$, for some even integer K, and let $u_0 = \frac{1}{2K}$. Then, the points of $\widetilde{\Lambda}_{\rm u} \cap \mathcal{V}_b$ are symmetrically located with respect to each BS of coordinate $b = 0, 1, \ldots, B-1$. $\lozenge$

A "user bin" $v(\mathcal{X})$, defined by the set of user locations $\mathcal{X} = \{x_0, x_1, \ldots, x_{m-1}\}$ with $x_i \in \widetilde{\Lambda}_{\rm u}$, is the collection of user location sets (indicated by "groups" in the following)

$$v(\mathcal{X}) = \{\{\mathcal{X} + c\} \ : \ c \in \Lambda_{\rm bs} \cap \mathcal{V}\}. \tag{3}$$

In particular, we choose $\mathcal{X}$ to be a symmetric set of points with respect to the positions of the BSs comprising cluster $\mathcal{C}$. The reason for this symmetry is two-fold: on one hand, a symmetric set generalizes the single location case and yet provides a set of statistically equivalent users (same set of distances from all BSs in the cluster), thus providing a richer system optimization parameter space. On the other hand, symmetry yields very simple closed-form expressions in the large-system analysis, by means of [11, Th. 3].

Example 5: In the 1-dimensional case of Example 1, we are interested in the cases $\mathcal{X} = \{-x, x\}$ and $\mathcal{X} = \{x, 1-x\}$, for some $x \in \widetilde{\Lambda}_{\rm u} \cap [0, 1/2]$, as shown in Fig. 2. This yields the bins

$$v(\{-x, x\}) = \{\{-x, x\}, \{1-x, 1+x\}, \ldots, \{B-1-x, B-1+x\}\}$$

and

$$v(\{x, 1-x\}) = \{\{x, 1-x\}, \{1+x, 2-x\}, \ldots, \{B-1+x, B-x\}\},$$

respectively. $\Diamond$

Cluster/group association and user group rate: The BSs forming a cluster are jointly coordinated by a "cluster controller" that collects all relevant channel state information and computes the beamforming coefficients for the desired MU-MIMO precoding scheme. For given sets $\{\mathcal{X}, \mathcal{C}\}$, the users in group $\mathcal{X}+c$ are served by the cluster $\mathcal{C}+c$, for all $c \in \Lambda_{\rm bs} \cap \mathcal{V}$ (see Fig. 2). By construction, each BS belongs to C clusters and transmits signals from all the C corresponding cluster controllers. These signals may share the same frequency band, or be defined on orthogonal subbands, depending on the system frequency reuse factor defined later in this section. There are mUN users in each group $\mathcal{X}+c$, and CMN jointly coordinated antennas in each cluster $\mathcal{C}+c$. We assume $mU \geq CM$, such that the downlink DoFs are always limited by the number of antennas.[4] The number of users effectively scheduled and served on each given slot is denoted by SN. We refer to these users as the "active users", and to the coefficient $S \in [0, CM]$ as the "loading factor". Depending on the geometry of $\mathcal{X}$ and $\mathcal{C}$ and on the type of beamforming used (see Section IV) S can be optimized for each pair $\{\mathcal{X}, \mathcal{C}\}$. We restrict to consider

[4]A system with $mU < CM$ is not fully loaded, in the sense that the infrastructure would support potentially a larger number of users.

schemes that serve an equal number SN/m of active users per location $x \in \mathcal{X}+c$. As anticipated before, by symmetry the users in the same bin are statistically equivalent. Therefore, without loss of generality, we may assume that a round-robin scheduling picks all subsets of size SN out of the whole mUN users in each group with the same fraction of time. In this way, the aggregate spectral efficiency of the group (indicated in the following a "group spectral efficiency") is shared evenly among all the users in the group.

Frequency reuse: The frequency reuse factor of the scheme is denoted by F. This can also be optimized for each given pair $\{\mathcal{X}, \mathcal{C}\}$. The system bandwidth is partitioned into F subbands of equal width. For $F = 1$, all clusters in $u(\mathcal{C})$ transmit on the whole system bandwidth. For $F > 1$, clusters are assigned different subbands according to a regular reuse pattern. For the 1-dimensional layout, any integer F dividing B is possible. For the 2-dimensional layout, we consider reuse factors given by $F = i^2+ij+j^2$ for non-negative integer i and j [38]. For later use, we define $\mathcal{D}(f)$ as the set of clusters active on subband $f \in \{0, \ldots, F-1\}$.

Example 6: Fig. 3 shows a 1-dimensional system with frequency reuse $F = 2$ for the clustering pattern of size $C = 2$ defined by $\mathcal{C} = \{0, 1\}$ and the user bin defined by $\mathcal{X} = \{x, 1-x\}$. Even-numbered clusters operate on subband 0 and odd-numbered clusters operate on subband 1. An example for the 2-dimensional hexagonal layout with $F = 3$ and $C = 1$ is shown in Fig. 1, where cells with the same color operate on the same subband. $\Diamond$

B. Channel statistics and received signal model

The average received signal power for a user located at $x \in \mathcal{V}$ from a BS antenna located at $b \in \mathcal{V}$ is denoted by $g(x, b)$, a polynomially decreasing function of the distance $d_\Lambda(x, b)$. The AWGN noise power spectral density is normalized to 1. For fixed For a given clustering pattern $u(\mathcal{C})$ and user bin $v(\mathcal{X})$, the fading channel coefficients from the CMN antennas of BS cluster $\mathcal{C} + c$ to an active user $k \in \{1, \ldots, S/m\}$ at location $x + c' : x \in \mathcal{X}$, on frequency subband f, form a random vector indicated by $\underline{\mathbf{h}}_{k,c',c}(f; x) \in \mathbb{C}^{CMN\times 1}$, with circularly-symmetric complex Gaussian entries, i.i.d. across the BS antennas, the subbands and the users (independent small-scale Rayleigh fading). In the considered network-MIMO schemes, active users are served with equal transmit power equal to $1/S$. Hence, the total transmit power per cluster is equal to N. Since each BS simultaneously participates in C clusters, also the total transmit power per BS is equal to N. Since we consider the limit for $N \to \infty$, the channel coefficients are normalized to have variance $1/N$, such that the received signal power is independent of N. This provides the correct scaling of the elements of the random channel matrices in

order to obtain the large-system limit results. We let the channel vector covariance matrix be given by $\mathbb{E}\left[\underline{\mathbf{h}}_{k,c',c}(f;x)\underline{\mathbf{h}}^{\mathsf{H}}_{k,c',c}(f;x)\right] = \frac{1}{N}\mathbf{G}_{c',c}(x)$, where $\mathbf{G}_{c',c}(x) = \text{diag}\left(g(x+c',b+c)\mathbf{I}_{MN} : b \in \mathcal{C}\right)$.[5] Notice that $\mathbf{G}_{c',c}(x)$ is independent of the user index k and on the subband index f, since the channels are identically distributed across subbands and co-located users.

Under the standard block-fading assumption [11]–[14], [18], the channel vectors are constant on each subband for blocks of length LN signal dimensions. Without loss of generality, we assume that these coherence blocks also correspond to the scheduling slot. Each slot is partitioned into an uplink training phase, of length $L_{\text{P}}N$ and a downlink data phase, of length $L_{\text{D}}N$. In this section we deal with the data phase, while the training phase is addressed in Section III. For the sake of notation simplicity, the slot "time" index is omitted: since we care about ergodic (average) rates, only the per-block marginal channel statistics matter. The data-bearing signal transmitted by cluster $\mathcal{C}+c$ on subband f is denoted by

$$\mathbf{X}_c(f) = \mathbf{U}_c(f)\mathbf{V}^{\mathsf{H}}_c(f) \tag{4}$$

where the matrix $\mathbf{U}_c(f) \in \mathbb{C}^{L_{\text{D}}N\times SN}$ contains the codeword (information-bearing) symbols arranged by columns. We assume that users' codebooks are drawn from an i.i.d. Gaussian random coding ensemble with symbols $\sim \mathcal{CN}(0,1/S)$. Achievable rates shall be obtained via the familiar *random coding argument* [39] with respect to this input distribution. The matrix $\mathbf{V}_c(f) \in \mathbb{C}^{CMN\times SN}$ contains the beamforming vectors arranged by columns, normalized to have unit norm. It is immediate to verify that, indeed, the average transmit power of any cluster $\mathcal{C}+c$, active on frequency f, is given by $\frac{1}{L_{\text{D}}N}\text{tr}\left(\mathbb{E}\left[\mathbf{X}^{\mathsf{H}}_c(f)\mathbf{X}_c(f)\right]\right) = N$, as desired.

Recalling the definition of $\mathcal{D}(f)$, the received signal for user k at location $x+c : x \in \mathcal{X}$ is given by

$$\mathbf{y}_{k,c}(f;x) = \sum_{c'\in\mathcal{D}(f)} \mathbf{U}_{c'}(f)\mathbf{V}^{\mathsf{H}}_{c'}(f)\underline{\mathbf{h}}_{k,c,c'}(f;x) + \mathbf{z}_{k,c}(f;x) \tag{5}$$

where $\mathbf{z}_{k,c}(f;x) \sim \mathcal{CN}\left(\mathbf{0},\frac{1}{F}\mathbf{I}_{L_{\text{D}}N}\right)$. Notice that a scheme using frequency reuse $F>1$ transmits with total cluster power N over a fraction $1/F$ of the whole system bandwidth. This is taken into account by letting the noise variance per component be equal to $1/F$, in the signal model (5).

By construction, the encoded data symbols for user k at location $x+c : x \in \mathcal{X}$, are the entries of the k-th column of $\mathbf{U}_c(f)$. The columns $k' \neq k$ of $\mathbf{U}_c(f)$ form the intra-cluster (multiuser) interference for user k. All other signals $\mathbf{U}_{c'}(f)$, with $c' \in \mathcal{D}(f), c' \neq c$, form the Inter-Cluster Interference (ICI). As

[5]We use $\text{diag}(\mathbf{M}_a : a \in \mathcal{A})$ to indicate a block-diagonal matrix with diagonal blocks $\mathbf{M}_a$, for some index a taking values in the ordered set $\mathcal{A}$, and $\mathbf{I}_n$ to indicate the $n\times n$ identity matrix.

seen in Section IV, intra-cluster interference and ICI are handled by a combination of beamforming and frequency reuse.

III. Uplink training and channel estimation

The CSIT is obtained on a per-slot basis, by letting all the scheduled (i.e., active) users in the slot sent pilot signals over the $L_{\mathrm{P}}N$ dimensions dedicated to uplink training.[6] We fix $\{\mathcal{X},\mathcal{C}\}$ and focus on the SN active users in the groups $\mathcal{X}+c : c \in \mathcal{D}(f)$. These users must send SN orthogonal pilot signals to allow channel estimation at their corresponding serving clusters $\mathcal{C}+c : c \in \mathcal{D}(f)$.

A. Pilot reuse scheme

Let $L_{\mathrm{P}} = QS$, where $Q \geq 1$ is an integer *pilot reuse factor* that can be optimized for each $\{\mathcal{X},\mathcal{C}\}$. Let $\mathbf{\Phi} \in \mathbb{C}^{QSN \times QSN}$ be a scaled unitary matrix, such that $\mathbf{\Phi}^{\mathsf{H}}\mathbf{\Phi} = \alpha_{\mathrm{ul}} QSN \mathbf{I}_{QSN}$, where α_{ul} denotes the uplink transmit power per user during the training phase. The columns of $\mathbf{\Phi}$ are partitioned into Q disjoint blocks of size SN columns each, denoted by $\mathbf{\Phi}_0, \ldots, \mathbf{\Phi}_{Q-1}$ and referred to as *training codebooks*. These are assigned to the groups in a periodic fashion, such that the same training codebook $\mathbf{\Phi}_q$ is reused every Q-th groups $\mathcal{X}+c : c \in \mathcal{D}(f)$. For later use, we let $q(c) \in \{0,\ldots,Q-1\}$ denote the index of the training codebook allocated to group $\mathcal{X}+c$, and define $\mathcal{P}(q,f) = \{c \in \mathcal{D}(f) : q(c) = q\}$ as the set of clusters active on subband f and using training codebook q. Pilot reuse is akin frequency reuse, but in general Q and F may be different in order to allow for additional flexibility in the system optimization.

Example 7: In the 1-dimensional layout with $C = 2$, $\mathcal{C} = \{0,1\}$ and $\mathcal{X} = \{x, 1-x\}$ we may have $F = 1$ (i.e., each cluster is active on the whole system bandwidth) and $Q = 2$ (i.e., two mutually orthogonal training codebooks are used alternately, such that the same set of uplink pilot signals is reused in every other cluster, as shown in Fig. 4). $\Diamond$

B. MMSE channel estimation and pilot contamination

The uplink signal received by the CMN antennas of cluster $\mathcal{C}+c : c \in \mathcal{D}(f)$, during the training phase, is given by

$$\mathbf{Y}_c(f) = \sum_{c' \in \mathcal{D}(f)} \mathbf{\Phi}_{q(c')} \underline{\mathbf{H}}^{\mathsf{H}}_{c',c}(f;\mathcal{X}) + \mathbf{Z}_c(f). \tag{6}$$

[6] As done in [18], also our analysis is slightly optimistic since it only accounts for the overhead and degradation due to uplink noisy channel estimation, while it assumes genie-aided overhead-free "dedicated training" to support coherent detection during data-transmission. As shown in [16], the effect of noisy dedicated training is minor relatively to the CSIT estimation error.

Because of TDD reciprocity, the *uplink* channel matrix $\underline{\mathbf{H}}_{c',c}(f;\mathcal{X}) \in \mathbb{C}^{CMN\times SN}$ contains the *downlink* channels $\underline{\mathbf{h}}_{k,c',c}(f;x)$ arranged by columns, for all active users $k=1,\ldots,SN/m$ at all locations $x+c' : x\in\mathcal{X}$. In (6), $\mathbf{Z}_c(f)\in\mathbb{C}^{L_{\mathrm{P}}\times CMN}$ denotes the uplink AWGN with components $\sim\mathcal{CN}(0,1)$. The goal of the uplink training phase is to provide to each cluster $\mathcal{C}+c$ an estimate of the channel vectors $\underline{\mathbf{h}}_{k,c,c}(f;x)$ for all the active users in the corresponding served group $\mathcal{X}+c$.

By projecting $\mathbf{Y}_c(f)$ onto the column of $\mathbf{\Phi}_{q(c)}$ associated to user k at location $x+c : x\in\mathcal{X}$ and dividing by $\alpha_{\mathrm{ul}}QSN$, the relevant observation for estimating the $\underline{\mathbf{h}}_{k,c,c}(f;x)$ is given by

$$\underline{\mathbf{r}}_{k,c}(f;x) = \sum_{c'\in\mathcal{P}(q(c),f)} \underline{\mathbf{h}}_{k,c',c}(f;x) + \underline{\mathbf{n}}_{k,c}(f) \tag{7}$$

where $\underline{\mathbf{n}}_{k,c}(f)\sim\mathcal{CN}(\mathbf{0},(\alpha^{\mathrm{ul}}QSN)^{-1}\mathbf{I}_{CMN})$. For any $c'\in\mathcal{P}(q(c),f)$, the MMSE estimate of $\underline{\mathbf{h}}_{k,c',c}(f;x)$ from $\underline{\mathbf{r}}_{k,c}(f;x)$ is obtained as

$$\widehat{\underline{\mathbf{h}}}_{k,c',c}(f;x) = \mathbf{G}_{c',c}(x)\left[(\alpha^{\mathrm{ul}}QS)^{-1}\mathbf{I}_{CMN} + \sum_{c''\in\mathcal{P}(q(c),f)}\mathbf{G}_{c'',c}(x)\right]^{-1}\underline{\mathbf{r}}_{k,c}(f;x) \tag{8}$$

Invoking the well-known MMSE decomposition, we can write

$$\underline{\mathbf{h}}_{k,c',c}(f;x) = \widehat{\underline{\mathbf{h}}}_{k,c',c}(f;x) + \underline{\mathbf{e}}_{k,c',c}(f;x), \tag{9}$$

where the channel estimate $\widehat{\underline{\mathbf{h}}}_{k,c',c}(f;x)$ and the error vector $\underline{\mathbf{e}}_{k,c',c}(f;x)$ are zero-mean uncorrelated jointly complex circularly symmetric Gaussian vectors (and therefore statistically independent due to joint Gaussianity). After some straightforward algebra (omitted for brevity), we obtain the covariance matrices $\mathbb{E}[\widehat{\underline{\mathbf{h}}}_{k,c',c}(f;x)\widehat{\underline{\mathbf{h}}}^{\mathsf{H}}_{k,c',c}(f;x)] = \frac{1}{N}\mathbf{\Xi}_{c',c}(x)$ and $\mathbb{E}[\underline{\mathbf{e}}_{k,c',c}(f;x)\underline{\mathbf{e}}^{\mathsf{H}}_{k,c',c}(f;x)] = \frac{1}{N}\mathbf{\Sigma}_{c',c}(x)$, where $\mathbf{\Xi}_{c',c}(x) = \mathrm{diag}\,(\xi_{c',c,b}(f;x)\mathbf{I}_{MN} : b\in\mathcal{C})$ and $\mathbf{\Sigma}_{c',c}(x) = \mathrm{diag}\,(\sigma_{c',c,b}(f;x)\mathbf{I}_{MN} : b\in\mathcal{C})$, and where we define

$$\sigma_{c',c,b}(f;x) = \frac{g(x+c',b+c)}{1+\gamma_{c',c,b}(f;x)} \tag{10}$$

$$\xi_{c',c,b}(f;x) = g(x+c',b+c) - \sigma_{c',c,b}(f;x) = \frac{g(x+c',b+c)}{1+\gamma_{c',c,b}(f;x)^{-1}} \tag{11}$$

with

$$\gamma_{c',c,b}(f;x) = \frac{g(x+c',b+c)}{(\alpha_{\mathrm{ul}}QS)^{-1}+\sum_{c''\in\mathcal{P}(q(c),f)\setminus c'}g(x+c'',b+c)} \tag{12}$$

The desired channel estimate at cluster $\mathcal{C}+c$ is given by $\widehat{\underline{\mathbf{h}}}_{k,c,c}(f;x)$, obtained by letting $c'=c$ in (8) – (12). Notice that the training phase observation $\underline{\mathbf{r}}_{k,c}(f;x)$ in (7) contains the superposition of all the channel vectors $\underline{\mathbf{h}}_{k,c',c}(f;x)$ of the users k at location $x+c' : x\in\mathcal{X}$, for all $c'\in\mathcal{P}(q(c),f)$, i.e., sharing the same pilot signal. This is the so-called *pilot contamination effect*, which is a major limiting factor

in the performance of TDD systems [18], [19]. Because of pilot contamination, the MMSE estimate $\widehat{\underline{\mathbf{h}}}_{k,c,c}(f;x)$ is *correlated* with the channels $\underline{\mathbf{h}}_{k,c',c}(f;x)$, for all $c' \in \mathcal{P}(q(c),f)$.

Next, we express the channel vector $\underline{\mathbf{h}}_{k,c',c}(f;x)$ for $c' \in \mathcal{P}(q(c),f)$ in terms of the estimate $\widehat{\underline{\mathbf{h}}}_{k,c,c}(f;x)$ and a component independent of $\widehat{\underline{\mathbf{h}}}_{k,c,c}(f;x)$. This decomposition is useful to proof the main results of Theorems 1, 2 and 3 in Section IV-B and it is the key to understand qualitatively the pilot contamination effect. From (8), and since $\mathbf{\Sigma}_{c,c}(x)$ is invertible, we have

$$\begin{aligned}\widehat{\underline{\mathbf{h}}}_{k,c',c}(f;x) &= \mathbb{E}\left[\underline{\mathbf{h}}_{k,c',c}(f;x)|\underline{\mathbf{r}}_{k,c}(f;x)\right] \\ &= \mathbf{G}_{c',c}(x)\mathbf{G}_{c,c}^{-1}(x)\widehat{\underline{\mathbf{h}}}_{k,c,c}(f;x). \end{aligned} \tag{13}$$

Using (9) into (13), the channel vector $\underline{\mathbf{h}}_{k,c',c}(f;x)$ from the antennas of cluster $\mathcal{C}+c$ to the *unintended* user k at location $x+c' : x \in \mathcal{X}$ can be written as

$$\underline{\mathbf{h}}_{k,c',c}(f;x) = \mathbf{G}_{c',c}(x)\mathbf{G}_{c,c}^{-1}(x)\widehat{\underline{\mathbf{h}}}_{k,c,c}(f;x) + \underline{\mathbf{e}}_{k,c',c}(f;x). \tag{14}$$

Joint Gaussianity, the mutual orthogonality of $\widehat{\underline{\mathbf{h}}}_{k,c',c}(f;x)$ and $\underline{\mathbf{e}}_{k,c',c}(f;x)$ and the fact that all covariance matrices are diagonal imply that $\widehat{\underline{\mathbf{h}}}_{k,c,c}(f;x)$ and $\underline{\mathbf{e}}_{k,c',c}(f;x)$ are mutually independent.

As anticipated before, (14) reveals qualitatively the pilot contamination effect. With LSUBF, as in [18], cluster $\mathcal{C}+c$ serves user k at location $x+c$ with beamforming vector $\widehat{\underline{\mathbf{h}}}_{k,c,c}(f;x)/\|\widehat{\underline{\mathbf{h}}}_{k,c,c}(f;x)\|$, which is strongly correlated with the channel vector $\underline{\mathbf{h}}_{k,c',c}(f;x)$ towards the unintended user k at location $x+c'$, sharing the same pilot signal. It follows that some constant amount of interfering power, that does not vanish with $N \to \infty$, is sent in the "spatial direction" of this user, leading to an interference limited system, as exactly quantified by Theorem 1 in Section IV-B. For the family of LZFBF schemes considered in this work, the pilot contamination effect is less intuitive, and it is precisely quantified by Theorems 2 and 3 in Section IV-B.

IV. MU-MIMO Precoders and Achievable Rates

In the family of network-MIMO schemes considered in this work, the beamforming matrix $\mathbf{V}_c(f)$ is calculated as a function of the estimated channel matrix $\widehat{\underline{\mathbf{H}}}_{c,c}(f;\mathcal{X})$. The schemes differ by the type of beamforming employed. In particular, we consider LZFBF where any active user k at location $x+c : x \in \mathcal{X}$, imposes ZF constraints on $J \geq 0$ clusters. A ZF constraint consists of the set of linear equations

$$\mathbf{v}_{j,c'}^{\mathsf{H}}(f;x')\widehat{\underline{\mathbf{h}}}_{k,c,c'}(f;x) = 0, \quad \forall \ (j,x',c') \neq (k,x,c) \tag{15}$$

where $\mathbf{v}_{j,c'}(f;x')$ denotes the column of $\mathbf{V}_{c'}(f)$ corresponding to user j at location $x'+c' : x' \in \mathcal{X}$.

A. Beamforming

Next we provide expressions for the cluster precoders for different choice of the parameter J.

Case $J = 0$**:** In this case no ZF constraints are imposed. Hence, we have

$$\mathbf{V}_c(f) = \mathrm{UNorm}\left\{\widehat{\mathbf{H}}_{c,c}(f;\mathcal{X})\right\} \tag{16}$$

where the operation UNorm$\{\cdot\}$ indicates a scaling of the columns of the matrix argument such that they have unit norm. It is immediate to see that (16) coincides with the Linear Single-User Beamforming (LSUBF) considered in [18].

Case $J = 1$**:** In this case any active user imposes ZF constraints on its own serving cluster. This yields the classical single-cluster LZFBF, for which

$$\mathbf{V}_c(f) = \mathrm{UNorm}\left\{\widehat{\mathbf{H}}^{+}_{c,c}(f;\mathcal{X})\right\}, \tag{17}$$

where

$$\mathbf{M}^{+} = \mathbf{M}\left[\mathbf{M}^{\mathsf{H}}\mathbf{M}\right]^{-1} \tag{18}$$

denotes the Moore-Penrose pseudo-inverse of the full column-rank matrix $\mathbf{M}$. It follows that $\mathbf{v}_{k,c}(f;x)$ is orthogonal to the estimated channels $\widehat{\underline{\mathbf{h}}}_{j,c,c}(f;x')$ for all other active users $(j,x') \neq (k,x)$ in the same cluster $\mathcal{C}+c$, i.e., ZF is used to tackle intra-cluster interference, but nothing is done with respect to ICI.

Case $J > 1$**:** In this case, beyond the ZF constraints imposed to the serving cluster, each user imposes additional ZF constraints to $J-1$ neighboring clusters in order to mitigate the ICI. Mitigating ICI through the beamforming design provides an alternative approach to frequency reuse and, in general, might be used jointly with frequency reuse. Let's focus on cluster $\mathcal{C}+c$. This is subject to ZF constraints imposed by its own users (i.e., users in group $\mathcal{X}+c$), as well as by some users at some locations $x'+c' : x' \in \mathcal{X}$ for $J-1$ neighboring clusters $c' \neq c$. In order to enable such constraints, the c-th cluster controller must be able to estimate the channels of these out-of-cluster users. This can be done if these users employ training codebooks with indices $q \neq q(c)$. In particular, $J > 1$ can be used only if the pilot reuse factor Q is larger than 1. In some cases, only the channel subvectors to the nearest BS in the cluster can be effectively estimated, since there are other users sharing the same pilot signal that are received with a stronger path coefficient. Then, the channel subvectors that cannot be estimated are treated as zero. Since these schemes are complicated to explain in full generality, we shall illustrate two specific examples, the generalization of which is cumbersome but conceptually straightforward, and can be worked out by the reader if interested in other specific cases.

Example 8: Consider Fig. 5(a), illustrating a 1-dimensional system with $\mathcal{C} = \{0, 1\}$, $\mathcal{X} = \{x, 1-x\}$, $F = 1$ and $Q = 2$. The beamforming matrix of each cluster c satisfies ZF constraints for its own served users and for the users in the $m = 2$ locations at minimum distance in the nearest neighbor clusters, $c-1$ and $c+1$. These locations collectively use distinct columns of the training codebooks $q \neq q(c)$. In the specific example, the reference cluster $c = 0$ uses training codebook $\mathbf{\Phi}_0$, and the nearest locations on the left and on the right of cluster 0 use the first $SN/2$ columns and the second $SN/2$ columns of the other training codebook $\mathbf{\Phi}_1$, respectively. Hence, cluster 0 controller can estimate all the channels of its own active users, at locations $x, 1-x$, and of the users in adjacent locations $-x$ and $1+x$, as shown in the figure. The beamforming matrix in the case of Fig. 5(a) is obtained as follows. Define

$$\mathbf{M}_c(f; \mathcal{X}) = \Big[\underbrace{\underline{\widehat{\mathbf{H}}}_{c,c}(f; \mathcal{X})}_{2MN \times SN} \Big| \underbrace{\underline{\widehat{\mathbf{H}}}_{c-1,c}(f; \{1-x\})}_{2MN \times SN/2} \Big| \underbrace{\underline{\widehat{\mathbf{H}}}_{c+1,c}(f; \{x\})}_{2MN \times SN/2} \Big] \tag{19}$$

be the matrix of dimension $2MN \times 2SN$ of all estimated channels at cluster controller c, where the first block corresponds to the desired active users and the remaining blocks correspond to users in the adjacent clusters for which a ZF constraint is imposed. Then,

$$\mathbf{V}_c(f) = \left[\mathrm{UNorm} \left\{ \mathbf{M}_c^+(f; \mathcal{X}) \right\} \right]_{k=1}^{SN} \tag{20}$$

where $[\cdot]_n^m$ extracts the columns from n to m of the matrix argument. This scheme can be generalized to $J = Q$, where each cluster c satisfies ZF constraints for the desired SN active users in its own cluster and for a total of $(J-1)SN$ additional users in the nearest location of neighboring clusters. $\lozenge$

Example 9: Consider Fig. 5(b), illustrating the same 1-dimensional system as in Example 8 with a different beamforming design. In this case, the beamforming matrix of each cluster c satisfies ZF constraints for its own served users and *all* the users in the nearest neighbor clusters. However, some of these users share the same columns of the training codebooks $q \neq q(c)$. In the specific example, the reference cluster $c = 0$ uses training codebook $\mathbf{\Phi}_0$, and the clusters to the left and to the right the other training codebook $\mathbf{\Phi}_1$. Users at location $-1+x$ use the same pilot signals of users at location $1+x$, and users at location $-x$ use the same pilot signals of users at location $2-x$. Then the 0-th cluster controller assumes that the channel coefficients for BSs at larger distance are equal to zero. In the example, for locations $-1+x$ and $-x$, only the subvector of dimension MN corresponding to the antennas of BS 0 is estimated, while the remaining subvector to BS 1 is treated as zero. Similarly, for locations $1+x$ and $2-x$ only the subvector of dimension MN corresponding to the antennas of BS 1 is estimated, while the remaining subvector to BS 0 is treated as zero.

The beamforming matrix corresponding to the scheme of Fig. 5(b) is obtained as follows. Define

$$\mathbf{M}_c(f;\mathcal{X}) = \Big[\underbrace{\widehat{\underline{\mathbf{H}}}_{c,c}(f;\mathcal{X})}_{2MN\times SN}\Big|\underbrace{\widehat{\underline{\mathbf{H}}}_{c-1,c}(f;\mathcal{X})}_{2MN\times SN}\odot\mathbf{L}\Big|\underbrace{\widehat{\underline{\mathbf{H}}}_{c+1,c}(f;\mathcal{X})}_{2MN\times SN/2}\odot\mathbf{R}\Big] \tag{21}$$

be the matrix of dimension $2MN \times 3SN$ of all estimated channels at cluster controller c, where $\odot$ indicates elementwise product and where

$$\mathbf{L} = \begin{bmatrix} \mathbf{1}_{MN\times SN} \\ \mathbf{0}_{MN\times SN} \end{bmatrix}, \quad \mathbf{R} = \begin{bmatrix} \mathbf{0}_{MN\times SN} \\ \mathbf{1}_{MN\times SN} \end{bmatrix}$$

are masking matrices that null out the subvectors of the channels that are treated as zero in the beamforming design. Then, $\mathbf{V}_c(f)$ is again given by (20) although in this case $\mathbf{M}_c(f;\mathcal{X})$ is given by (21) instead of (19). This scheme can be generalized to $J = C(Q-1)+1$, where each cluster c satisfies ZF constraints for the desired SN active users in its own cluster and for a total of $(J-1)SN$ additional users in the neighboring clusters, with some channel sub-vectors set to zero. $\Diamond$

B. Achievable group spectral efficiency

Letting $R_{k,c}^{(N)}(f;x)$ denote the spectral efficiency (in bit/s/Hz) of user k at location $x+c : x \in \mathcal{X}$, served by cluster c according to a scheme as defined above, we define the group spectral efficiency of bin $v(\mathcal{X})$ as

$$R_{\mathcal{X},\mathcal{C}}(F,C,J) = \frac{1}{FBN}\sum_{f=0}^{F-1}\sum_{c\in\Lambda_{\rm bs}\cap\mathcal{V}}\sum_{x\in\mathcal{X}}\sum_{k=1}^{SN/m} R_{k,c}^{(N)}(f;x) \tag{22}$$

In Appendices A and B, we prove the following results.

Theorem 1: For given sets $\mathcal{X},\mathcal{C}$, and system parameters F,S and Q, in the limit of $N\to\infty$, the following group spectral efficiency of bin $v(\mathcal{X})$ is achievable with LSUBF precoding ($J=0$):

$$R_{\mathcal{X},\mathcal{C}}(F,C,J=0) \;=\; \frac{S}{mF}\sum_{x\in\mathcal{X}}\log\left(1+\frac{\frac{CM}{S}\underline{\xi}_{0,0}(x)}{\frac{1}{F}+\eta(x)+\frac{CM}{S}\zeta(x)}\right), \tag{23}$$

where[7]

$$\eta(x) = \frac{1}{mC}\sum_{x'\in\mathcal{X}}\sum_{b\in\mathcal{C}}\sum_{c\in\mathcal{D}(0)}\frac{\xi_{c,c,b}(x')g(x,c+b)}{\underline{\xi}_{c,c}(x')} \tag{24}$$

and

$$\zeta(x) = \sum_{c\in\mathcal{P}(0,0)\setminus 0}\frac{1}{\underline{\xi}_{c,c}(x)}\left(\frac{1}{C}\sum_{b\in\mathcal{C}}\frac{g(x,c+b)}{g(x,b)}\xi_{c,c,b}(x)\right)^2, \tag{25}$$

[7]In (24) and (25) it is assumed, without loss of generality, that cluster $c=0$ uses subband $f=0$ and training codebook $q=0$.

with

$$\underline{\xi}_{c,c}(x) = \frac{1}{C}\sum_{b\in\mathcal{C}} \xi_{c,c,b}(x), \tag{26}$$

are coefficients that depend uniquely on the system geometry, frequency and pilot reuse, but are independent of the loading factor S and of the BS antenna factor M. ■

As a corollary of Theorem 1, we can recover the result of [18]. It is sufficient to let $M \to \infty$ in (23) and obtain the regime of infinite number of BS antennas per active user. Particularizing this for fixed S, $C = 1$, and $Q = 1$ as in [18], the group spectral efficiency becomes

$$\lim_{M\to\infty} R_{\mathcal{X},\{0\}}(F, 1, 0) = \frac{S}{mF}\sum_{x\in\mathcal{X}} \log\left(1 + \frac{g(x,0)^2}{\sum_{c\in\mathcal{P}(0,0)\setminus 0} g(x,c)^2}\right) \tag{27}$$

As observed in [18], in this regime the system spectral efficiency is uniquely limited by the ICI due to pilot contamination.

The next result yields the achievable group spectral efficiency of LZFBF in the case of single-cell processing (i.e., for $C = 1$). We define $\mathcal{E}(x)$ as the set of $J-1$ clusters $c \neq 0$ with centers closest to $x \in \mathcal{X}$ (if $J = 1$ then $\mathcal{E}(x) = \emptyset$). Then, we have:

Theorem 2: For given set $\mathcal{X}$, $C = 1$ (i.e., $\mathcal{C} = \{0\}$), and system parameters F, S and Q, in the limit of $N \to \infty$, the following group spectral efficiency of bin $v(\mathcal{X})$ is achievable with LZFBF precoding ($J \geq 1$):

$$R_{\mathcal{X},\{0\}}(F, 1, J \geq 1) = \frac{S}{mF}\sum_{x\in\mathcal{X}} \log\left(1 + \frac{\frac{M-JS}{S}\xi_{0,0,0}(x)}{\frac{1}{F} + \alpha(x) + \frac{M-JS}{S}\beta(x)}\right) \tag{28}$$

where

$$\alpha(x) = \sum_{c\in\mathcal{P}(0,0)\cup\mathcal{E}(x)} \sigma_{0,c,0}(x) + \sum_{c\in\mathcal{D}(0)-\mathcal{P}(0,0)-\mathcal{E}(x)} g(x,c) \tag{29}$$

and

$$\beta(x) = \sum_{c\in\mathcal{P}(0,0)\setminus 0} \left(\frac{g(x,c)}{g(x,0)}\right)^2 \xi_{c,c,0}(x) \tag{30}$$

are coefficients that depend uniquely on the system geometry, frequency and pilot reuse, but are independent of the loading factor S and of the BS antenna factor M. ■

In passing, we notice that the limit of (28) for $M \to \infty$, coincides with (27). Therefore, as observed in [18], in the "Massive MIMO" regime LZFBF yields no advantage over the simpler LSUBF.

The case of LZFBF with multicell processing ($C > 1$) needs some more notation. First, as illustrated in Examples 8 and 9, we consider the cases $J = 1$, $J = Q$ and $J = C(Q-1)+1$, referred to as cases (a), (b) and (c), respectively, for the sake of brevity. In case (c) it is useful to define $b(x, c) =$

$\arg\min\{d_\Lambda(x, c+b) : b \in \mathcal{C}\}$, i.e., the closest BS to location $x \in \mathcal{X}$ in cluster $c \in \mathcal{E}(x)$. For $C > 1$, an exact asymptotic ICI power expression cannot be found due to the complicated statistical dependence of beamforming vectors and channel vectors due to pilot contamination. However, the following result yields an achievable rate based on an upper bound on the ICI power (see details in Appendix B):

Theorem 3: For given sets $\mathcal{X}, \mathcal{C}$ with $C > 1$, and system parameters F, S and Q, in the limit of $N \to \infty$, the following group spectral efficiency of bin $v(\mathcal{X})$ is achievable with LZFBF precoding ($J \geq 1$):

$$R_{\mathcal{X},\mathcal{C}}(F, C, J \geq 1) = \frac{S}{mF} \sum_{x \in \mathcal{X}} \log\left(1 + \frac{\frac{CM-JS}{S}\underline{\xi}_{0,0}(x)}{\frac{1}{F} + \underline{\alpha}(x) + \frac{CM}{S}\underline{\beta}(x)}\right) \tag{31}$$

where

$$\underline{\alpha}(x) = \begin{cases} \displaystyle\sum_{c \in \mathcal{E}(x) \cup \{0\}} \underline{\sigma}_{0,c}(x) + \sum_{c \in \mathcal{D}(0) \setminus 0 - \mathcal{E}(x)} \underline{g}_{0,c}(x), & \text{in cases (a) and (b),} \\ \underline{\sigma}_{0,0}(x) + \displaystyle\sum_{c \in \mathcal{D}(0) \setminus 0 - \mathcal{E}(x)} \underline{g}_{0,c}(x) + & \\ + \dfrac{1}{C} \displaystyle\sum_{c \in \mathcal{E}(x)} \left(\sigma_{0,c,b(x,c)}(x) + \sum_{b \in \mathcal{C} \setminus b(x,c)} g(x, c+b)\right) & \text{in case (c),} \end{cases} \tag{32}$$

and

$$\underline{\beta}(x) = \sum_{c \in \mathcal{P}(0,0) \setminus 0} \frac{1}{C} \sum_{b \in \mathcal{C}} \left(\frac{g(x, c+b)}{g(x, b)}\right)^2 \xi_{c,c,b}(x), \tag{33}$$

with

$$\underline{g}_{0,c}(x) = \frac{1}{C} \sum_{b \in \mathcal{C}} g(x, c+b), \quad \underline{\sigma}_{0,c}(x) = \frac{1}{C} \sum_{b \in \mathcal{C}} \sigma_{0,c,b}(x), \tag{34}$$

are coefficients that depend uniquely on the system geometry, frequency and pilot reuse, but are independent of the loading factor S and of the BS antenna factor M. ■

V. Scheduling and Fairness

Consider a system with K bins, $\{v(\mathcal{X}_0), \ldots, v(\mathcal{X}_{K-1})$, defined by sets $\mathcal{X}_k$ of symmetric locations chosen to uniformly discretize the cellular coverage region $\mathcal{V}$. The net bin spectral efficiency in bit/s/Hz, for each bin $v(\mathcal{X}_k)$, is obtained by maximizing over all possible schemes in the family, i.e., over all possible clusters $\mathcal{C}$ of size $C = 1, 2, \ldots$, frequency reuse factor F, loading factor S, pilot reuse factor Q, and beamforming scheme indicated by J, the product

$$\max\{1 - QS/L, 0\} \times R_{\mathcal{X}_k,\mathcal{C}}(F, C, J) \tag{35}$$

where the first term takes into account the pilot dimensionality overhead, and the second term is the spectral efficiency of the data phase for a given network-MIMO scheme, given by Theorems 1, 2 or 3, depending on the case. The maximization of (35) is subject to the constraint $JS \leq CM$, which becomes relevant for $J > 0$ (i.e., for LZFBF precoding). Maximizing (35) requires searching over a discrete parameter space (apart from S, which is continuous). The simple closed-form expressions given in Theorems 1, 2 and 3 allow for an efficient system optimization, avoiding lengthy Monte Carlo simulations.

Suppose that for each bin $v(\mathcal{X}_k)$, the best scheme in the family of network-MIMO schemes is found, and let $R^\star(\mathcal{X}_k)$ denote the corresponding maximum of (35). Then, a scheduler allocates the different bins on the time-frequency slots in order to maximize some desired network utility function of the user rates. With randomized or round-robin selection of the active users in each bin, each user in bin $v(\mathcal{X}_k)$ shares on average an equal fraction of the product $\rho_k R^\star(\mathcal{X}_k)$, where ρ_k is the fraction of time-frequency slots allocated to bin $v(\mathcal{X}_k)$. Under the assumption that users in the same bin should be treated with equal priority, we can focus on the maximization of a componentwise non-decreasing concave network utility function of the bin spectral efficiencies, denoted by $\mathcal{G}(R_0, \ldots, R_{K-1})$. The scheduler determines the fractions $\{\rho_k\}$ by solving the following convex problem:

$$\begin{aligned} \text{maximize} \quad & \mathcal{G}(R_0, \ldots, R_{K-1}) \\ \text{subject to} \quad & R_k \leq \rho_k R^\star(\mathcal{X}_k), \\ & \sum_{k=0}^{K-1} \rho_k \leq 1, \quad \rho_k \geq 0. \end{aligned} \tag{36}$$

For example, if Proportional Fairness (PF) [30] is desired, we have

$$\mathcal{G}(R_0, \ldots, R_{K-1}) = \sum_{k=0}^{K-1} \log R_k, \tag{37}$$

resulting in the bin time-frequency sharing fractions $\rho_k = 1/K$ (each bin is given an equal amount of slots). In contrast, if the minimum user rate is relevant, we can impose max-min fairness by considering the function

$$\mathcal{G}(R_0, \ldots, R_{K-1}) = \min_{k=0,\ldots,K-1} R_k. \tag{38}$$

This results in the bin time-frequency sharing fractions $\rho_k = \frac{\frac{1}{R^\star(\mathcal{X}_k)}}{\sum_{j=0}^{K-1} \frac{1}{R^\star(\mathcal{X}_j)}}$. More in general, a whole family of scheduling rules including (37) and (38) as special cases is obtained by using the so-called α-fairness network utility function, as defined in [29].

VI. Numerical Results and Discussion

In this section, we present some illustrative numerical results showing the following facts: 1) the asymptotic large-system analysis yields a very accurate approximation of the performance (obtained by monte Carlo simulation) of actual finite-dimensional systems; 2) the proposed architecture based on partitioning the users' population in homogeneous bins and serving each bin with specifically tailored network-MIMO scheme provides significant gains with respect to the "Massive MIMO" scheme of [18], in the relevant regime of a finite number of BS antennas per active user.

At this point, it is worthwhile to make a comment on the convergence of finite-dimensional systems to the large-system limit as $N \to \infty$. The approach of analyzing multiuser communication systems affected by random parameters (such as random channel matrices or random spreading matrices in CDMA) in the limit of large dimension in order to exploit the rich, powerful and elegant theory of limiting distributions of large random matrices [20] was pioneered in [40], [41] in the case of random-spreading CDMA, and successfully applied to single-user MIMO channels (see for example [42]–[45]) and to network-MIMO cellular systems [11], [21], [33]–[35]. It was observed experimentally and proved mathematically (e.g., see [22], [23]) that the convergence of the actual finite-dimensional system spectral efficiency to the corresponding large-system limit is very fast, as the system dimension N increases. In particular, well-known techniques can be used to analyze the "fluctuation" of the quantities of interest around their large-system limit for large but finite N. Typically, finite-N "concentration" results are analogous to the Central Limit Theorem for i.i.d. random variables, but the convergence is much faster owing to the fact that the eigenvalues of the matrices appearing in the spectral efficiency expressions are strongly correlated (see for example the discussion of the results in [23]). Since this convergence analysis is standard but cumbersome, and invariably points out that the large-system results are very good predictions of the actual performance in cases of practical interest, here we focused only on the limit for $N \to \infty$ and provided a comparison with finite-dimensional simulation in order to corroborate our claims.

Fig. 6 shows the group spectral efficiency in (35) as a function of the bin locations within a cell for different schemes identified by the parameters (F, C, J) and Q. The group spectral efficiency is obtained by Monte Carlo simulation (dotted) and and is compared against the corresponding values from the closed-form large-system analysis (solid), for the 1-dimensional cell layout of Fig. 2 with $B = 24$ BSs, $M = 30$ antenna factor per BS, $L = 40$ coherence block dimension factor, and $K = 10$ bins in each cluster, where clusters and location bins are given in Example 3 and 5, with x uniformly distributed in $[0, 1/2]$. The pathloss model is the same as in [28], where $g(x, b) = G_0/(1 + (d_\Lambda(x, b)/\delta)^\alpha)$, with

$G_0 = 10^6$, $\alpha = 3.76$, and $\delta = 0.05$, and reflects (after suitable normalizations) a typical cellular scenario with 1km diameter cells in a sub-urban environment. The (1,1,1) scheme with $Q = 1$ yields the best performance for locations near the cell center. However, at the cell edges, $C = 2$, $J = 2$, or $F = 2$ (not included in the figure) attains significantly better performance. As anticipated above, the limit for $N \to \infty$ matches very accurately with the Monte Carlo simuation even for very small N (we used the minimum possible $N = 1$ in this case). For this reason, in the following we present only the results for the large-system limit, obtained using the closed-form expressions of Theorems 1, 2 and 3.

In the 2-dimensional case, we considered the layout with $B = 19$ hexagonal cells as shown in Fig. 1. For comparison, we assume the same system model as in [18], with channel coherence block dimension, the cell radius, and pathloss model given by $L_{\mathrm{P}} = 84$, 1.6 km, and $g(x, b)$ in the same form as before, with parameters $G_0 = 10^6$, $\delta = 0.1$ km, and $\alpha = 3.8$, respectively. Log-normal shadowing, considered in [18], is not considered here (see the comment in Section VII). We considered schemes with cluster size $C = 1$ and $C = 3$, $K = 16$ bins with 48 user locations, where the cluster and bin layout are qualitatively described in Fig. 2. The frequency reuse factor F and pilot reuse factor Q are selected between 1 and 3 and, when F or $Q = 3$, the frequency subbands or training codebooks are allocated to clusters as shown in Fig. 1 where different colors denotes different subbands or training codebooks. Fig. 7 illustrates the optimum over the family of network-MIMO schemes for (a) $M = 20$ and (b) $M = 100$. In both cases, $(1, 1, 1)$ is optimal in the inner part of the cell, but schemes with $(3, 3, 1)$ or $(3, 1, 1)$ yield better performance for locations near cell boundary. We notice also that the inner area within which the (1,1,1) scheme is the best increases with the BS antenna factor M.

Next, we compare the performance of the proposed architecture with the one advocated in [18]. Fig. 8 shows the bin-optimized spectral efficiency normalized by the spectral efficiency of $(1, 1, 0), Q = 1$ scheme (corresponding to [18]), under two-dimensional layout with $M = 50$. The gain of the proposed architecture ranges from about 40% to 580%, depending on the users' location. Fig. 9 shows the system throughput as a function of M in the two-dimensional layout. The throughput obtained for fixed parameters in the considered family of network-MIMO schemes, as well as for the bin-optimized mixed-mode letting the scheduler choose the bin and the associate network-MIMO scheme as described in Section V is shown, and compared with the reference performance of the $(1, 1, 0), Q = 1$ scheme. The cluster scheme includes two cases where the cluster pattern is fixed as one of two shown in Fig. 2 or can be switched to the closest one depending on the user locations. The system throughput of Fig. 9 is obtained under PF scheduling (see (37)). For the sake of comparison, we assumed 20 MHz bandwidth and the coherence block size $L = 84$ as in [18] (considering the parameters of 3GPP LTE TDD system).

As the figure reveals, the $(3,3,1)$ schemes perform very well for small $M < 20$ while, as M increases, the $(1,1,1)$ scheme is best. The bin-optimized architecture improves the throughput further at any value of M. The dotted horizontal line in Fig. 9 denotes the cell throughput claimed in [18] in the limit of an infinite number of transmit antennas per user with the $(1,1,0), Q = 1$ scheme. We notice that this limit can be approached very slowly, and more than 10000 antennas per BS are required (clearly impractical). For finite number of antennas, the proposed architecture achieves the same throughput of the scheme in [18] with a 10-fold reduction in the number of antennas at the base stations (roughly, from 500 to 50 antennas, as indicated by the arrow).

VII. Conclusions

We studied a novel network-MIMO TDD architecture that achieves spectral efficiencies comparable with the recently proposed "Massive MIMO" scheme, with one order of magnitude less antennas per active user per cell. The proposed strategy operates by partitioning the users population into geographically determined "bins". The time-frequency scheduling slots are allocated to the bins in order to form independent MU-MIMO transmissions, each of which is optimized for the corresponding bin. This strategy allows the uplink training reuse factor, the frequency reuse factor, the active user loading factor, the BS cooperative cluster size and the type of MU-MIMO linear beamforming to be finely tailored to the particular user bin. We considered system optimization over 1-dimensional and 2-dimensional cell layouts, based on a family of network-MIMO schemes ranging from single-cell processing to joint processing over clusters of coordinated BSs, with linear precoders ranging from conventional linear single-user beamforming to zero-forcing beamforming with additional zero-forcing constraints for neighboring cells. In order to carry out the system optimization, we developed efficient closed-form expressions for the achievable spectral efficiency for each scheme in the family and each bin in the cellular layout. Our closed-form analysis is based on the large-system limit, where all system dimensions scale to infinity with fixed ratios, and make use of recent results (by some of the authors of this paper) on the analysis of cellular systems with linear zero-forcing beamforming and channel estimation errors [11]. The performance predicted by the large-system asymptotic analysis is shown to match very well with finite-dimensional simulations. Our numerical results show that different schemes in the considered family achieve the best spectral efficiency at different user locations. This suggests the need for a location-adaptive scheme selection to serve efficiently the whole coverage region. The resulting overall system is therefore a "mixed-mode" network-MIMO architecture, where different schemes, each of which is optimized for the corresponding user bin, are multiplexed in the time-frequency plane.

As a final remark, it is worthwhile to point out that the approach of partitioning the users in homogeneous sets, serving each set according to a specifically optimized scheme, and using a scheduler to multiple different schemes in order to maximize some desired network utility function, can be generalized to the case of shadowing, and to the case of users with different mobility. This generalization is, however, non-trivial. For example, in the presence of slow frequency-flat shadowing, "bins" are no-longer uniquely determined by the users geographic position. Rather, the set of large-scale channel gains (including shadowing), should be used to classify the users in equivalence classes. Also, in the presence of users with different mobility, users should be classified also on the basis of their different channel coherence block length. The issue of how to optimally cluster users into equivalence classes that can be efficiently served in parallel, by MU-MIMO spatial multiplexing, represents an interesting and important problem for future work.

APPENDIX A
PROOF OF THEOREM 1

We focus on the reference cluster $\mathcal{C}$ (i.e., $c = 0$), with corresponding served group of locations $\mathcal{X} = \{x_0, \ldots, x_{m-1}\}$. For the sake of notation simplicity, we omit the subchannel index f, and let $\mathcal{D}$ denote the set of clusters active on the same subchannel of cluster 0, and $\mathcal{P}$ denote the set of clusters that share the same pilot block as cluster 0. From (5), the (scalar) signal received at some symbol interval of the data phase, at the k-th active user receiver at location $x \in \mathcal{X}$, is given by

$$
\begin{aligned}
y_{k,0}(x) \;=\; & u_{k,0}(x)\mathbf{v}_{k,0}^{\mathsf{H}}(x)\underline{\mathbf{h}}_{k,0,0}(x) && \text{(39a)}\\
& + \sum_{j\neq k} u_{j,0}(x)\mathbf{v}_{j,0}^{\mathsf{H}}(x)\underline{\mathbf{h}}_{k,0,0}(x) + \sum_{x'\in\mathcal{X}\setminus x}\sum_{j} u_{j,0}(x')\mathbf{v}_{j,0}^{\mathsf{H}}(x')\underline{\mathbf{h}}_{k,0,0}(x) && \text{(39b)}\\
& + \sum_{c'\in\mathcal{D}\setminus 0}\sum_{x'\in\mathcal{X}}\sum_{j} u_{j,c'}(x')\mathbf{v}_{j,c'}^{\mathsf{H}}(x')\underline{\mathbf{h}}_{k,0,c'}(x) + z_{k,0}(x), && \text{(39c)}
\end{aligned}
$$

where $u_{j,c'}(x')$ denotes the code symbol transmitted by cluster c', to user j at location $x' + c' : x' \in \mathcal{X}$. With LSUBF downlink precoding, we have

$$
\mathbf{v}_{j,c'}(x') = \left\| \widehat{\underline{\mathbf{h}}}_{j,c',c'}(x') \right\|^{-1} \widehat{\underline{\mathbf{h}}}_{j,c',c'}(x') \tag{40}
$$

Using the MMSE decomposition (9), we isolate the *useful signal term* from (39a), given by,

$$
u_{k,0}(x)\mathbf{v}_{k,0}^{\mathsf{H}}(x)\widehat{\underline{\mathbf{h}}}_{k,0,0}(x). \tag{41}
$$

The sum of the residual self-interference term due to the channel estimation error with the signals in (39b) transmitted by cluster 0 to the other users, results in the *intra-cluster interference term*

$$u_{k,0}(x)\mathbf{v}_{k,0}^{\mathsf{H}}(x)\underline{\mathbf{e}}_{k,0,0}(x)+\sum_{j\neq k}u_{j,0}(x)\mathbf{v}_{j,0}^{\mathsf{H}}(x)\underline{\mathbf{h}}_{k,0,0}(x)+\sum_{x'\in\mathcal{X}\setminus x}\sum_{j}u_{j,0}(x')\mathbf{v}_{j,0}^{\mathsf{H}}(x')\underline{\mathbf{h}}_{k,0,0}(x). \tag{42}$$

Finally, the *ICI term* and background noise are given in (39c).

A standard achievability bound based on the worst-case uncorrelated additive noise [15] yields that the achievable rate

$$R_{k,0}^{(N)}(x)=\mathbb{E}\left[\log\left(1+\frac{\mathbb{E}\left[|\text{useful signal term}|^2\mid\widehat{\underline{\mathbf{h}}}_{k,0,0}(x)\right]}{\mathbb{E}\left[|\text{noise plus interference term}|^2\mid\widehat{\underline{\mathbf{h}}}_{k,0,0}(x)\right]}\right)\right]. \tag{43}$$

Both numerator and denominator of the Signal-to-Interference plus Noise Ratio (SINR) appearing inside the log in (43) converge to deterministic limits as $N\to\infty$. We will use extensively the representation of the channel MMSE estimates as

$$\widehat{\underline{\mathbf{h}}}_{j,c,c'}(x') \;=\; \frac{1}{\sqrt{N}}\boldsymbol{\Xi}_{c,c'}^{1/2}(x')\mathbf{a}_{j,c,c'}(x') \tag{44}$$

where the vectors $\mathbf{a}_{j,c,c'}(x')$ are i.i.d. $\sim\mathcal{CN}(\mathbf{0},\mathbf{I}_{CMN})$, with generic components denoted by $\{a_{n,b}:n=1,\ldots,MN\}$ for all $b\in\mathcal{C}$. We will also make use of the following limit, which follows as a direct application of the strong law of large numbers:

$$\left\|\widehat{\underline{\mathbf{h}}}_{j,c,c'}(x')\right\|^2=\sum_{b\in\mathcal{C}}\xi_{c,c',b}(x')\frac{1}{N}\sum_{n=1}^{MN}|a_{n,b}|^2\overset{\text{a.s.}}{\to}CM\underline{\xi}_{c,c'}(x') \tag{45}$$

where $\underline{\xi}_{c,c'}(x')$ is defined in (26). Using (40), the SINR numerator is given by

$$\begin{aligned}\mathbb{E}\left[\left|u_{k,0}(x)\mathbf{v}_{k,0}^{\mathsf{H}}(x)\widehat{\underline{\mathbf{h}}}_{k,0,0}(x)\right|^2\middle|\widehat{\underline{\mathbf{h}}}_{k,0,0}(x)\right] &= \mathbb{E}\left[|u_{k,0}(x)|^2\left\|\widehat{\underline{\mathbf{h}}}_{k,0,0}(x)\right\|^2\middle|\widehat{\underline{\mathbf{h}}}_{k,0,0}(x)\right] &\text{(46a)}\\ &= \frac{1}{S}\left\|\widehat{\underline{\mathbf{h}}}_{k,0,0}(x)\right\|^2 &\text{(46b)}\\ &\overset{\text{a.s.}}{\to} \frac{CM}{S}\underline{\xi}_{0,0}(x) &\text{(46c)}\end{aligned}$$

where in (46a) we used the LSUBF definition (40).

Next, we notice that all the terms forming interference and noise are uncorrelated. Hence, the conditional average interference power can be calculated as a sum of individual terms. The self-interference due to non-ideal CSIT is given by

$$\begin{aligned}\mathbb{E}\left[\left|u_{k,0}(x)\mathbf{v}_{k,0}^{\mathsf{H}}(x)\underline{\mathbf{e}}_{k,0,0}(x)\right|^2\middle|\widehat{\underline{\mathbf{h}}}_{k,0,0}(x)\right] &= \frac{1}{SN}\|\widehat{\underline{\mathbf{h}}}_{k,0,0}(x)\|^{-2}\widehat{\underline{\mathbf{h}}}_{k,0,0}^{\mathsf{H}}(x)\boldsymbol{\Sigma}_{0,0}(x)\widehat{\underline{\mathbf{h}}}_{k,0,0}(x)\\ &= \frac{1}{SN}\frac{\sum_{b\in\mathcal{C}}\xi_{0,0,b}(x)\sigma_{0,0,b}(x)\frac{1}{N}\sum_{n=1}^{MN}|a_{n,b}|^2}{CM\underline{\xi}_{0,0}(x)}\\ &\overset{\text{a.s.}}{\to} 0 &\text{(47)}\end{aligned}$$

where (47) follows from noticing that

$$\sum_{b\in\mathcal{C}} \xi_{0,0,b}(x)\sigma_{0,0,b}(x)\frac{1}{N}\sum_{n=1}^{MN}|a_{n,b}|^2 \overset{\text{a.s.}}{\to} M\sum_{b\in\mathcal{C}}\xi_{0,0,b}(x)\sigma_{0,0,b}(x),$$

which is a finite constant.

Following very similar calculations (omitted for brevity) and recalling that $g(x,b)=\xi_{0,0,b}(x)+\sigma_{0,0,b}(x)$ (see (11)) and that SN/m users per location $x'\in\mathcal{X}$ are active, we obtain the intra-cluster interference power terms as

$$\frac{1}{mC}\sum_{x'\in\mathcal{X}}\sum_{b\in\mathcal{C}}\frac{\xi_{0,0,b}(x')g(x,b)}{\underline{\xi}_{0,0}(x')} \tag{48}$$

Next, we consider the ICI power term. In doing so, we must pay attention to the pilot contamination effect. In particular, we have to separate all contributions in (39c) coming from the k-th beam of clusters $c'\in\mathcal{P}$ (i.e., for users sharing the same pilot signal of the reference user k at $x\in\mathcal{X}$), from the rest. The two contributions to the ICI are

$$\mathcal{I}_{\text{same pilot}} = \sum_{c'\in\mathcal{P}\setminus 0} u_{k,c'}(x)\mathbf{v}_{k,c'}^{\mathsf{H}}(x)\underline{\mathbf{h}}_{k,0,c'}(x) \tag{49}$$

and

$$\begin{aligned}\mathcal{I}_{\text{no same pilot}} &= \sum_{c'\in\mathcal{P}\setminus 0}\sum_{j\neq k} u_{j,c'}(x)\mathbf{v}_{j,c'}^{\mathsf{H}}(x)\underline{\mathbf{h}}_{k,0,c'}(x) + \sum_{c'\in\mathcal{P}\setminus 0}\sum_{x'\in\mathcal{X}\setminus x}\sum_{j} u_{j,c'}(x')\mathbf{v}_{j,c'}^{\mathsf{H}}(x')\underline{\mathbf{h}}_{k,0,c'}(x)\\ &\quad+\sum_{c'\in\mathcal{D}-\mathcal{P}}\sum_{x'\in\mathcal{X}}\sum_{j} u_{j,c'}(x')\mathbf{v}_{j,c'}^{\mathsf{H}}(x')\underline{\mathbf{h}}_{k,0,c'}(x)\end{aligned} \tag{50}$$

Both $\mathcal{I}_{\text{same pilot}}$ and $\mathcal{I}_{\text{no same pilot}}$ are independent of $\widehat{\underline{\mathbf{h}}}_{k,0,0}(x)$. Therefore, conditioning in the expectation can be omitted. Each individual term appearing in the sum (50) yields

$$\begin{aligned}N\mathbb{E}\left[\left|u_{j,c'}(x')\mathbf{v}_{j,c'}^{\mathsf{H}}(x')\underline{\mathbf{h}}_{k,0,c'}(x)\right|^2\right] &\to \frac{1}{S}\frac{\frac{1}{N}\text{tr}\left(\mathbf{\Xi}_{c',c'}(x')\mathbf{G}_{0,c'}(x)\right)}{CM\underline{\xi}_{c',c'}(x')}\\ &= \frac{1}{SC}\sum_{b\in\mathcal{C}}\frac{\xi_{c',c',b}(x')g(x,c'+b)}{\underline{\xi}_{c',c'}(x')}.\end{aligned}$$

Summing over all terms, we have

$$\mathbb{E}\left[|\mathcal{I}_{\text{no same pilot}}|^2\right] = \sum_{c'\in\mathcal{D}\setminus 0}\frac{1}{mC}\sum_{x'\in\mathcal{X}}\sum_{b\in\mathcal{C}}\frac{\xi_{c',c',b}(x')g(x,c'+b)}{\underline{\xi}_{c',c'}(x')}. \tag{51}$$

In order to evaluate $\mathbb{E}\left[|\mathcal{I}_{\text{same pilot}}|^2\right]$, we use the decomposition (14) applied to $\underline{\mathbf{h}}_{k,0,c'}(x)$, namely,

$$\underline{\mathbf{h}}_{k,0,c'}(x) = \mathbf{G}_{0,c'}(x)\mathbf{G}_{c',c'}^{-1}(x)\widehat{\underline{\mathbf{h}}}_{k,c',c'}(x) + \underline{\mathbf{e}}_{k,0,c'}(x). \tag{52}$$

The general term in (49) yields

$$\begin{aligned}
&\mathbb{E}\left[\left|u_{k,c'}(x)\mathbf{v}^{\mathsf{H}}_{k,c'}(x)\underline{\mathbf{h}}_{k,0,c'}(x)\right|^2\right] \\
&= \frac{1}{S}\mathbb{E}\Big[\|\widehat{\underline{\mathbf{h}}}_{k,c',c'}(x)\|^{-2}\left(\widehat{\underline{\mathbf{h}}}^{\mathsf{H}}_{k,c',c'}(x)\mathbf{G}_{0,c'}(x)\mathbf{G}^{-1}_{c',c'}(x)\widehat{\underline{\mathbf{h}}}_{k,c',c'}(x)\right)^2 \\
&\quad + \widehat{\underline{\mathbf{h}}}^{\mathsf{H}}_{k,c',c'}(x)\underline{\mathbf{e}}_{k,0,c'}(x)\underline{\mathbf{e}}^{\mathsf{H}}_{k,0,c'}(x)\widehat{\underline{\mathbf{h}}}_{k,c',c'}(x)\Big] \\
&\to \frac{M}{SC\underline{\xi}_{c',c'}(x)}\left(\sum_{b\in\mathcal{C}}\frac{g(x,c'+b)}{g(x,b)}\xi_{c',c',b}(x)\right)^2
\end{aligned} \tag{53}$$

where, inside the expectation, we used the a.s. limits (45),

$$\begin{aligned}
\widehat{\underline{\mathbf{h}}}^{\mathsf{H}}_{k,c',c'}(x)\mathbf{G}_{0,c'}(x)\mathbf{G}^{-1}_{c',c'}(x)\widehat{\underline{\mathbf{h}}}_{k,c',c'}(x) &= \sum_{b\in\mathcal{C}}\frac{g(x,c'+b)}{g(c'+x,c'+b)}\xi_{c',c',b}(x)\frac{1}{N}\sum_{n=1}^{MN}|a_{n,b}|^2 \\
&\overset{\text{a.s.}}{\to} M\sum_{b\in\mathcal{C}}\frac{g(x,c'+b)}{g(x,b)}\xi_{c',c',b}(x),
\end{aligned}$$

with $g(c'+x,c'+b)=g(x,b)$, and $\widehat{\underline{\mathbf{h}}}^{\mathsf{H}}_{k,c',c'}(x)\underline{\mathbf{e}}_{k,0,c'}(x) \overset{a.s.}{\to} 0$, and the limit

$$\begin{aligned}
\mathbb{E}\left[\widehat{\underline{\mathbf{h}}}^{\mathsf{H}}_{k,c',c'}(x)\underline{\mathbf{e}}_{k,0,c'}(x)\underline{\mathbf{e}}^{\mathsf{H}}_{k,0,c'}(x)\widehat{\underline{\mathbf{h}}}_{k,c',c'}(x)\right] &= \frac{1}{N}\mathbb{E}\left[\widehat{\underline{\mathbf{h}}}^{\mathsf{H}}_{k,c',c'}(x)\boldsymbol{\Sigma}_{0,c'}(x)\widehat{\underline{\mathbf{h}}}_{k,c',c'}(x)\right] \\
&= \frac{1}{N^2}\mathrm{tr}\left(\boldsymbol{\Xi}_{c',c'}(x)\boldsymbol{\Sigma}_{0,c'}(x)\right)\to 0
\end{aligned} \tag{54}$$

Summing over all such terms, we obtain

$$\mathbb{E}\left[|\mathcal{I}_{\text{same pilot}}|^2\right] = \frac{CM}{S}\sum_{c'\in\mathcal{P}\setminus 0}\frac{1}{\underline{\xi}_{c',c'}(x)}\left(\frac{1}{C}\sum_{b\in\mathcal{C}}\frac{g(x,c'+b)}{g(x,b)}\xi_{c',c',b}(x)\right)^2 \tag{55}$$

Using (46c), (48), (51) and (55) in (43), recalling that the noise variance is equal to $1/F$, summing over all users in the reference group $\mathcal{X}$ and observing that the system is symmetric (by construction) with respect to any cluster and any subband, we find the normalized group spectral efficiency of bin $v(\mathcal{X})$ in the form (23).

APPENDIX B
PROOF OF THEOREMS 2 AND 3

With reference to Section IV-A, we consider LZFBF with or without inter-cluster interference (ICI) constraints, depending on the value of $J \geq 1$. In particular, each cluster creates JSN beamforming vectors for SN users in the same cluster and $(J-1)SN$ users in the neighboring clusters. Any active user in the system, at any given scheduling slot, imposes ZF constraints (see (15)) to J clusters. We restrict our attention to the three cases treated in Section IV-A, again referred to as cases (a) $J=1$; (b)

$J = Q$; and (c) $J = (Q-1)C + 1$. As before, we focus on the reference cluster $\mathcal{C}$ ($c = 0$) with served group $\mathcal{X}$. In such cases, the beamforming matrix $\mathbf{V}_0$ is given by the column-normalized Moore-Penrose pseudo-inverse of the estimated channel matrix (see (17), (19) and (21)), of size $CMN \times JSN$. This matrix is formed by blocks of size $N \times SN/m$, in the form:

$$\mathbf{M}_0 = \begin{bmatrix} \mathbf{M}_{0,0} & \mathbf{M}_{0,1} & \cdots & \mathbf{M}_{0,Jm-1} \\ \mathbf{M}_{1,0} & \mathbf{M}_{1,1} & \cdots & \mathbf{M}_{1,Jm-1} \\ \vdots & & & \vdots \\ \mathbf{M}_{CM-1,0} & \mathbf{M}_{CM-1,1} & \cdots & \mathbf{M}_{CM-1,Jm-1} \end{bmatrix}, \tag{56}$$

where each block $\mathbf{M}_{i,j}$ corresponds to the MN antennas of BS $b \in \mathcal{C}$ and to the SN/m active users in some location x' with respect to which ZF constraints are imposed. For the purpose of analysis, it is important to notice that the blocks $\mathbf{M}_{i,j}$ are mutually independent, and each block contains i.i.d. elements with mean zero and variance that depends on the block. For example, if block $\mathbf{M}_{i,j}$ corresponds to a user location $c' + x' : x' \in \mathcal{X}$ and BS $b \in \mathcal{C}$ such that the corresponding channel vectors are estimated from the uplink training phase, the elements of $\mathbf{M}_{i,j}$ are $\sim \mathcal{CN}(0, \xi_{c',0,b}(x)/N)$ (see (11) in Section III-B). Instead, if block $\mathbf{M}_{i,j}$ corresponds to a user location and a BS such that the corresponding channel vectors are treated as zero (see Section IV-A, Example 9), then $\mathbf{M}_{i,j} = \mathbf{0}$ (all-zero block).

The signal received by user k at location $x \in \mathcal{X}$ takes on the form (39). From [11, Theorem 3] the rate

$$R_{k,0}^{(N)}(x) = \mathbb{E}\left[\log\left(1 + \frac{\mathbb{E}\left[|\text{useful signal term}|^2 \mid \mathbf{v}_{k,0}(x), \widehat{\underline{\mathbf{h}}}_{k,0,0}(x)\right]}{\mathbb{E}\left[|\text{noise plus interference term}|^2 \mid \mathbf{v}_{k,0}(x), \widehat{\underline{\mathbf{h}}}_{k,0,0}(x)\right]}\right)\right] \tag{57}$$

is achievable, assuming that the receiver has perfect knowledge of its own estimated channel and beamforming vector. The large-system limit of the LZFBF useful signal coefficient $\mathbf{v}_{k,0}^{\mathsf{H}}(x)\widehat{\underline{\mathbf{h}}}_{k,0,0}(x)$ for channel matrices in the form (56) was obtained in [11, Theorem 1] (details are omitted for the sake of brevity). While in general this limit is obtained as the solution of a fixed-point equation that must be solved numerically, the user locations and the BS positions considered in this paper satisfy the symmetry conditions given in [11, Section III.A], and the asymptotic useful signal term admits a simple closed form given in [11, eq. (32)]. Applying this result we obtain

$$\left|\mathbf{v}_{j,c'}^{\mathsf{H}}(x')\widehat{\underline{\mathbf{h}}}_{j,c',c'}(x')\right|^2 \overset{\text{a.s.}}{\to} (CM - JS)\underline{\xi}_{c',c'}(x') \tag{58}$$

for any $j, c'\Lambda_{\text{bs}} \cap \mathcal{V}$ and $x' \in \mathcal{X}$. By construction, it is assumed that $JS < CM$. Notice the well-known dimensionality limit of the ZF beamforming: when the ratio of the number of ZF constraints per degree

of freedom (antenna) $JS/(CM)$ tends to 1, the effective useful signal term vanishes. Using (58) and recalling that $\mathbb{E}[|u_{k,0}(x)|^2] = 1/S$ we obtain the SINR numerator in (57) as

$$\mathbb{E}\left[\left|u_{k,0}(x)\mathbf{v}_{k,0}^{\mathsf{H}}(x)\widehat{\underline{\mathbf{h}}}_{k,0,0}(x)\right|^2 \middle| \mathbf{v}_{k,0}(x), \widehat{\underline{\mathbf{h}}}_{k,0,0}(x)\right] \overset{\text{a.s.}}{\to} \frac{CM - JS}{S}\underline{\xi}_{0,0}(x). \tag{59}$$

As done in Appendix A, we consider the intra-cluster, ICI and noise terms in the SINR denominator of (57) separately. The ZF constraints imply that $\mathbf{v}_{j,0}^{\mathsf{H}}(x')\widehat{\underline{\mathbf{h}}}_{k,0,0}(x) = 0$ for all $(j,x') \neq (k,x) : x' \in \mathcal{X}$. Therefore, the intra-cluster interference term given in general by (42), reduces to

$$\sum_{x'\in\mathcal{X}}\sum_{j} u_{j,0}(x')\mathbf{v}_{j,0}^{\mathsf{H}}(x')\underline{\mathbf{e}}_{k,0,0}(x),$$

and its conditional second moment is given by

$$\begin{aligned}
&\mathbb{E}\left[\left|\textstyle\sum_{x'\in\mathcal{X}}\sum_j u_{j,0}(x')\mathbf{v}_{j,0}^{\mathsf{H}}(x')\underline{\mathbf{e}}_{k,0,0}(x)\right|^2 \middle| \mathbf{v}_{k,0}(x), \widehat{\underline{\mathbf{h}}}_{k,0,0}(x)\right] \\
&= \frac{1}{S}\mathbb{E}\left[\text{tr}\left(\mathbf{V}_0^{\mathsf{H}}\mathbb{E}\left[\underline{\mathbf{e}}_{k,0,0}(x)\underline{\mathbf{e}}_{k,0,0}^{\mathsf{H}}(x)\right]\mathbf{V}_0\right)\middle|\mathbf{v}_{k,0}(x)\right] \\
&= \frac{1}{SN}\mathbb{E}\left[\text{tr}\left(\mathbf{V}_0\mathbf{V}_0^{\mathsf{H}}\mathbf{\Sigma}_{0,0}(x)\right)\middle|\mathbf{v}_{k,0}(x)\right] \\
&\overset{\text{a.s.}}{\to} \frac{1}{C}\sum_{b\in\mathcal{C}}\sigma_{0,0,b}(x) \triangleq \underline{\sigma}_{0,0}(x),
\end{aligned} \tag{60}$$

where the last line holds from the following lemma[8].

Lemma 1: If the user locations and BS positions are symmetric (in the sense defined in [11, Section III.A], which is satisfied for the choice of lattice-based user locations sets considered in this work), the matrix $\mathbf{V}_c\mathbf{V}_c^{\mathsf{H}}$ satisfies the "constant partial trace" property in the large-system limit, i.e., the sum of a block of MN consecutive diagonal elements of $\mathbf{V}_c\mathbf{V}_c^{\mathsf{H}}$ corresponding to the antennas of BS $b \in \mathcal{C}$, divided by SN, tends to the constant limit $1/C$, independent of the BS index b.

Proof: The sum of the b-th diagonal element block of size MN of $\mathbf{V}_c\mathbf{V}_c^{\mathsf{H}}$, divided by SN, is written as

$$\frac{1}{SN}\sum_{\ell=(b-1)MN+1}^{bMN}\left[\mathbf{V}_c\mathbf{V}_c^{\mathsf{H}}\right]_{\ell,\ell} = \frac{1}{SN}\sum_{\ell=(b-1)MN+1}^{bMN}\sum_{x\in\mathcal{X}}\sum_{j=1}^{SN/m}\left|[\mathbf{v}_{j,c}(x)]_\ell\right|^2, \tag{61}$$

where $[\mathbf{v}_{j,c}(x)]_\ell$ denotes the ℓ-th element of the column $\mathbf{v}_{j,c}(x)$ of $\mathbf{V}_c$. Next, for the sake of clarity, we identify some terms in the notation of this paper with the corresponding terms in the notation of [11, Lemma 1]. To this purpose, we enumerate the locations $x \in \mathcal{X}$ as $k = 1, \ldots, m$. The transmit power to

[8]Notice that since the columns of $\mathbf{V}_0$ have unit norm we have $\frac{1}{N}\text{tr}(\mathbf{V}_0\mathbf{V}_0^{\mathsf{H}}) = \frac{1}{N}\text{tr}(\mathbf{V}_0^{\mathsf{H}}\mathbf{V}_0) = S$. However, since $\mathbf{\Sigma}_{0,0}(x)$ is block-diagonal with constant diagonal blocks $\sigma_{0,0,b}(x)\mathbf{I}_{MN}$, the constant partial trace property is needed in order to obtain (60).

each active user in the cluster is $q_k = 1/S$ and the fraction of active users per location is $\mu_k = S/m$. Both quantities are constant with k. Also, the term

$$\frac{1}{N} \sum_{\ell=(b-1)MN+1}^{bMN} \sum_{j=1}^{SN/m} \left| [\mathbf{v}_{j,c}(x)]_\ell \right|^2,$$

coincides with the term $\theta_{b,k}$ defined in [11, eq. (26)] Therefore, the term in (61) can be written as $\frac{1}{S}\sum_{k=1}^{m} \theta_{b,k} = \sum_{k=1}^{m} q_k \theta_{b,k}$. Applying [11, Lemma 1], we have

$$\sum_{k=1}^{m} q_k \theta_{b,k} = \sum_{k=1}^{m/C} q_k \mu_k = \frac{m}{C} \cdot \frac{1}{S} \cdot \frac{S}{m} = \frac{1}{C}.$$

■

Next, we consider the ICI term and we separate it into $\mathcal{I}_{\text{same pilot}}$ and $\mathcal{I}_{\text{no same pilot}}$. The conditioning with respect to $\mathbf{v}_{k,0}(x), \widehat{\mathbf{h}}_{k,0,0}(x)$ is irrelevant for the ICI terms and therefore it can be omitted. First, we evaluate the pilot contamination effect for the case $C = 1$. Using (52), (59) and (49), we obtain

$$\begin{aligned}
\mathbb{E}\left[\left| \mathcal{I}_{\text{same pilot}} \right|^2 \right] &= \mathbb{E}\left[\left| \sum_{c' \in \mathcal{P}\setminus 0} u_{k,c'}(x) \mathbf{v}_{k,c'}^{\mathsf{H}}(x) \underline{\mathbf{h}}_{k,0,c'}(x) \right|^2 \right] \\
&= \frac{1}{S} \sum_{c' \in \mathcal{P}\setminus 0} \mathbb{E}\left[\left| \mathbf{v}_{k,c'}^{\mathsf{H}}(x) \left(\mathbf{G}_{0,c'}(x) \mathbf{G}_{c',c'}^{-1}(x) \widehat{\underline{\mathbf{h}}}_{k,c',c'}(x) + \underline{\mathbf{e}}_{k,0,c'}(x) \right) \right|^2 \right] \\
&= \frac{1}{S} \sum_{c' \in \mathcal{P}\setminus 0} \left\{ \left(\frac{g(x,c')}{g(x,0)} \right)^2 \mathbb{E}\left[\left| \mathbf{v}_{k,c'}^{\mathsf{H}}(x) \widehat{\underline{\mathbf{h}}}_{k,c',c'}(x) \right|^2 \right] + \mathbb{E}\left[\left| \mathbf{v}_{k,c'}^{\mathsf{H}}(x) \underline{\mathbf{e}}_{k,0,c'}(x) \right|^2 \right] \right\} \\
&\to \frac{M - JS}{S} \sum_{c' \in \mathcal{P}\setminus 0} \left(\frac{g(x,c')}{g(x,0)} \right)^2 \underline{\xi}_{c',c'}(x) \qquad (62)
\end{aligned}$$

where we used (58) and

$$\begin{aligned}
\mathbb{E}\left[\left| \mathbf{v}_{k,c'}^{\mathsf{H}}(x) \underline{\mathbf{e}}_{k,0,c'}(x) \right|^2 \right] &= \frac{1}{N} \mathbb{E}\left[\mathbf{v}_{k,c'}^{\mathsf{H}}(x) \mathbf{\Sigma}_{0,c'}(x) \mathbf{v}_{k,c'}(x) \right] \\
&\leq \frac{1}{N} \mathbb{E}\left[\|\mathbf{v}_{k,c'}(x)\|^2 \right] \max_{b \in \mathcal{C}} \{\sigma_{0,c',b}(x)\} \\
&= \frac{1}{N} \max_{b \in \mathcal{C}} \{\sigma_{0,c',b}(x)\} \to 0 \qquad (63)
\end{aligned}$$

For $C > 1$, we have $\mathbf{G}_{0,c'}(x)\mathbf{G}_{c',c'}^{-1}(x) = \text{diag}\left(\frac{g(x,c'+b)}{g(x,b)} \mathbf{I}_{MN} : b \in \mathcal{C} \right)$. While $\mathbf{v}_{k,c'}^{\mathsf{H}}(x)$ and $\widehat{\underline{\mathbf{h}}}_{k,c',c'}(x)$ are orthogonal by design, the term $\mathbb{E}\left[\left| \mathbf{v}_{k,c'}^{\mathsf{H}}(x) \mathbf{G}_{0,c'}(x) \mathbf{G}_{c',c'}^{-1}(x) \widehat{\underline{\mathbf{h}}}_{k,c',c'}(x) \right|^2 \right]$ is generally non-zero and does not admit a simple closed-form since $\mathbf{v}_{k,c'}(x)$ and $\widehat{\underline{\mathbf{h}}}_{k,c',c'}(x)$ are statistically dependent. In order to overcome this problem, we consider the following upper bound obtained by applying Cauchy-Schwartz inequality:

$$\left| \mathbf{v}_{k,c'}^{\mathsf{H}}(x) \mathbf{G}_{0,c'}(x) \mathbf{G}_{c',c'}^{-1}(x) \widehat{\underline{\mathbf{h}}}_{k,c',c'}(x) \right|^2 \leq \|\mathbf{v}_{k,c'}(x)\|^2 \left\| \mathbf{G}_{0,c'}(x) \mathbf{G}_{c',c'}^{-1}(x) \widehat{\underline{\mathbf{h}}}_{k,c',c'}(x) \right\|^2 \qquad (64)$$

Recalling that $\mathbf{v}_{k,c'}(x)$ has unit norm and that $\mathbb{E}[\widehat{\underline{\mathbf{h}}}_{k,c',c'}(x)\widehat{\underline{\mathbf{h}}}^{\mathsf{H}}_{k,c',c'}(x)] = \frac{1}{N}\mathbf{\Xi}_{c',c'}(x)$, we obtain

$$\mathbb{E}\left[\left|\mathcal{I}_{\text{same pilot}}\right|^2\right] \leq \frac{CM}{S}\sum_{c'\in\mathcal{P}\setminus 0}\frac{1}{C}\sum_{b\in\mathcal{C}}\left(\frac{g(x,c'+b)}{g(x,b)}\right)^2\xi_{c',c',b}(x) \tag{65}$$

Next, we examine the ICI power caused by the term $\mathcal{I}_{\text{no same pilot}}$. In the case of $J \geq 2$, this can be further decomposed into a term $\mathcal{I}_{\text{ICI-ZF}}$, taking into account the clusters which have a ZF constraint with respect to user k at location $x \in \mathcal{X}$, and $\mathcal{I}_{\text{no-ICI-ZF}}$, taking into account all other clusters. In order to proceed, we define $\mathcal{E}(x)$ as the set of $J-1$ clusters $c \neq 0$ with centers closest to $x \in \mathcal{X}$. With these definition, we have

$$\mathcal{I}_{\text{ICI-ZF}} = \sum_{c'\in\mathcal{E}(x)}\sum_{x'\in\mathcal{X}}\sum_{j} u_{j,c'}(x')\mathbf{v}^{\mathsf{H}}_{j,c'}(x')\underline{\mathbf{h}}_{k,0,c'}(x) \tag{66}$$

and

$$\begin{aligned}\mathcal{I}_{\text{no-ICI-ZF}} = &\sum_{c'\in\mathcal{P}\setminus 0}\sum_{j\neq k} u_{j,c'}(x)\mathbf{v}^{\mathsf{H}}_{j,c'}(x)\underline{\mathbf{h}}_{k,0,c'}(x) + \sum_{c'\in\mathcal{P}\setminus 0}\sum_{x'\in\mathcal{X}\setminus x}\sum_{j} u_{j,c'}(x')\mathbf{v}^{\mathsf{H}}_{j,c'}(x')\underline{\mathbf{h}}_{k,0,c'}(x)\\ &+ \sum_{c'\in\mathcal{D}-\mathcal{P}-\mathcal{E}(x)}\sum_{x'\in\mathcal{X}}\sum_{j} u_{j,c'}(x')\mathbf{v}^{\mathsf{H}}_{j,c'}(x')\underline{\mathbf{h}}_{k,0,c'}(x).\end{aligned} \tag{67}$$

We start with the terms in (67). For $c' \in \mathcal{P}\setminus 0$, by definition of LZFBF we have that $\mathbf{v}^{\mathsf{H}}_{j,c'}(x')\widehat{\underline{\mathbf{h}}}_{k,c',c'}(x) = 0$ for all $(j,x') \neq (k,x)$. For $C=1$, since $\mathbf{G}_{0,c'}(x)\mathbf{G}^{-1}_{c',c'}(x)$ is a scaled identity matrix, using (52) we have that

$$\mathbf{v}^{\mathsf{H}}_{j,c'}(x')\underline{\mathbf{h}}_{k,0,c'}(x) = \mathbf{v}^{\mathsf{H}}_{j,c'}(x')\underline{\mathbf{e}}_{k,0,c'}(x) \tag{68}$$

For $c' \in \mathcal{D}-\mathcal{P}-\mathcal{E}(x)$, the vectors $\mathbf{v}^{\mathsf{H}}_{j,c'}(x')$ and $\underline{\mathbf{h}}_{k,0,c'}(x)$ are statistically independent. Hence, for $C=1$ we have

$$\begin{aligned}&\lim_{N\to\infty}\mathbb{E}\left[\left|\mathcal{I}_{\text{no-ICI-ZF}}\right|^2\right]\\ &= \lim_{N\to\infty}\left\{\sum_{c'\in\mathcal{P}\setminus 0}\frac{1}{SN}\mathbb{E}\left[\text{tr}\left(\mathbf{V}_{c'}\mathbf{V}^{\mathsf{H}}_{c'}\mathbf{\Sigma}_{0,c'}(x)\right)\right] + \sum_{c'\in\mathcal{D}-\mathcal{P}-\mathcal{E}(x)}\frac{1}{SN}\mathbb{E}\left[\text{tr}\left(\mathbf{V}_{c'}\mathbf{V}^{\mathsf{H}}_{c'}\mathbf{G}_{0,c'}(x)\right)\right]\right\}\\ &= \sum_{c'\in\mathcal{P}\setminus 0}\sigma_{0,c',0}(x) + \sum_{c'\in\mathcal{D}-\mathcal{P}-\mathcal{E}(x)} g(x,c')\end{aligned} \tag{69}$$

where in (69) we used Lemma 1 for matrix $\mathbf{V}_{c'}\mathbf{V}^{\mathsf{H}}_{c'}$.

For $C > 1$, because of the block-diagonal form of the matrix $\mathbf{G}_{0,c'}(x)\mathbf{G}^{-1}_{c',c'}(x)$ already mentioned before, (68) does not hold in general. An upper bound to the interference power in this case can be obtained by assuming that the MMSE estimate $\widehat{\underline{\mathbf{h}}}_{k,0,c'}(x)$ of the channel from user k at location $x \in \mathcal{X}$

and the antennas of cluster c' is so noisy that it can be considered equal to zero. Therefore, the estimation error $\mathbf{e}_{k,0,c'}(x)$ has covariance $\frac{1}{N}\mathbf{G}_{0,c'}(x)$, and we obtain

$$\lim_{N\to\infty} \mathbb{E}\left[\left|\mathcal{I}_{\text{no-ICI-ZF}}\right|^2\right] \leq \sum_{c'\in\mathcal{D}\setminus 0-\mathcal{E}(x)} \underline{g}_{0,c'}(x) \tag{70}$$

where $\underline{g}_{0,c'}(x)$ is defined in (34). Finally, we consider $\mathcal{I}_{\text{ICI-ZF}}$ in (66). We distinguish different cases depending on the value of J. In case (a), this term is zero. In case (b), we have $\mathbf{v}_{j,c'}^{\mathsf{H}}(x')\widehat{\underline{\mathbf{h}}}_{k,0,c'}(x) = 0$ for all j and all $x \in \mathcal{E}(x)$. Hence, similarly to (60), we obtain

$$\mathbb{E}\left[\left|\mathcal{I}_{\text{ICI-ZF}}\right|^2\right] \;\to\; \sum_{c'\in\mathcal{E}(x)} \underline{\sigma}_{0,c'}(x) \tag{71}$$

In case (c), the ZF vectors $\mathbf{v}_{j,c'}(x')$ of cluster $c' \in \mathcal{E}(x)$ are calculated by imposing orthogonality conditions with the segment of the estimated channel vector $\widehat{\underline{\mathbf{h}}}_{k,0,c'}(x)$ corresponding to the MN antennas of the closest BS. In order to proceed further, we define the index of the closest BS to location x in cluster $c' \in \mathcal{E}(x)$ as $b(x,c) = \arg\min\{d_\Lambda(x, c+b) : b \in \mathcal{C}\}$. Then, the effective channel used for ZF beamforming calculation is given by

$$\widetilde{\underline{\mathbf{h}}}_{k,0,c'}(x) = \mathbf{\Psi}_{b(x,c')}\widehat{\underline{\mathbf{h}}}_{k,0,c'}(x)$$

where $\mathbf{\Psi}_{b(x,c')}$ is a selection matrix, with all elements equal to zero but for a block of diagonal elements corresponding to the positions of the MN antennas of BS $b(x,c')$. By construction, and using the MMSE decomposition, we have

$$\begin{aligned}
\mathbf{v}_{j,c'}^{\mathsf{H}}(x')\underline{\mathbf{h}}_{k,0,c'}(x) &= \mathbf{v}_{j,c'}^{\mathsf{H}}(x')\left(\mathbf{\Psi}_{b(x,c')}\widehat{\underline{\mathbf{h}}}_{k,0,c'}(x) + (\mathbf{I}_{CMN} - \mathbf{\Psi}_{b(x,c')})\widehat{\underline{\mathbf{h}}}_{k,0,c'}(x) + \mathbf{e}_{k,0,c'}(x)\right) \\
&= \mathbf{v}_{j,c'}^{\mathsf{H}}(x')\left((\mathbf{I}_{CMN} - \mathbf{\Psi}_{b(x,c')})\underline{\mathbf{h}}_{k,0,c'}(x) + \mathbf{\Psi}_{b(x,c')}\mathbf{e}_{k,0,c'}(x)\right) \\
&= \mathbf{v}_{j,c'}^{\mathsf{H}}(x')\widetilde{\mathbf{e}}_{k,0,c'}(x)
\end{aligned} \tag{72}$$

where $\widetilde{\mathbf{e}}_{k,0,c'}(x)$ is independent of all beamfomrming vectors $\mathbf{V}_{c'}$ of cluster $c' \in \mathcal{E}(x)$, and has covariance matrix

$$\frac{1}{N}\left((\mathbf{I}_{CMN} - \mathbf{\Psi}_{b(x,c')})\mathbf{G}_{0,c'}(x)(\mathbf{I}_{CMN} - \mathbf{\Psi}_{b(x,c')}) + \mathbf{\Psi}_{b(x,c')}\mathbf{\Sigma}_{0,c'}(x)\mathbf{\Psi}_{b(x,c')}\right)$$

Using these facts and operating similarly as in (71), we obtain

$$\mathbb{E}\left[\left|\mathcal{I}_{\text{ICI-ZF}}\right|^2\right] \;\to\; \sum_{c'\in\mathcal{E}(x)} \frac{1}{C}\left(\sum_{b\in\mathcal{C}\setminus b(x,c')} g(x, b+c') + \sigma_{0,c',b(x,c')}(x)\right) \tag{73}$$

From (59), (60), (62), (69), (71), and (73), the normalized group spectral efficiency for $C = 1$ and $J \geq 1$ is obtained in the form (28) For the cluster case $C > 1$, using bounds (65), and (70), we obtain the achievable normalized group spectral efficiency given by (31).[9]

[9]A lower bound to an achievable rate is also achievable.

REFERENCES

[1] 3GPP technical specification group radio access network, "Further advancements for E-UTRA: LTE-Advanced feasibility studies in RAN WG4," 3GPP TR 36.815, Tech. Rep., Mar. 2010.

[2] G. Boudreau, J. Panicker, N. Guo, R. Chang, N. Wang, and S. Vrzic, "Interference coordination and cancellation for 4G networks," *IEEE Commun. Mag.*, vol. 47, no. 4, pp. 74–81, Apr. 2009.

[3] H. Dahrouj and W. Yu, "Coordinated beamforming for the multicell multi-antenna wireless system," *IEEE Trans. on Wireless Commun.*, vol. 9, no. 5, pp. 1748–1759, May 2010.

[4] H. Huh, H. C. Papadopoulos, and G. Caire, "Multiuser MISO transmitter optimization for intercell interference mitigation," *IEEE Trans. on Sig. Proc.*, vol. 58, no. 8, pp. 4272–4285, Aug. 2010.

[5] G. J. Foschini, K. Karakayali, and R. A. Valenzuela, "Coordinating multiple antenna cellular networks to achieve enormous spectral efficiency," *IEE Proc. Commun.*, vol. 153, no. 4, pp. 548–555, Aug 2006.

[6] S. Jing, D. N. C. Tse, J. B. Soriaga, J. Hou, J. E. Smee, and R. Padovani, "Downlink macro-diversity in cellular networks," in *Proc. IEEE Int. Symp. on Inform. Theory (ISIT)*, Nice, France, June 2007.

[7] F. Boccardi and H. Huang, "Limited downlink network coordination in cellular networks," in *Proc. IEEE Int. Symp. on Personal, Indoor, and Mobile Radio Commun. (PIMRC)*, Athens, Greece, Sept. 2007.

[8] G. Caire, S. A. Ramprashad, H. C. Papadopoulos, C. Pepin, and C.-E. W. Sundberg, "Multiuser MIMO downlink with limited inter-cell cooperation: approximate interference alignment in time, frequency and space," in *Proc. Allerton Conf. on Commun., Control, and Computing*, Urbana-Champaign, IL, Sept. 2008.

[9] S. A. Ramprashad and G. Caire, "Cellular vs. network MIMO: a comparison including the channel state information overhead," in *Proc. IEEE Int. Symp. on Personal, Indoor, and Mobile Radio Commun. (PIMRC)*, Tokyo, Japan, Sept. 2009.

[10] S. A. Ramprashad, G. Caire, and H. C. Papadopoulos, "Cellular and network MIMO architectures: MU-MIMO spectral efficiency and costs of channel state information," in *Proc. IEEE Asilomar Conf. on Signals, Systems, and Computers (ACSSC)*, Pacific Grove, CA, Nov. 2009.

[11] H. Huh, A. M. Tulino, and G. Caire, "Network MIMO with linear zero-forcing beamforming: large system analysis, impact of channel estimation and reduced-complexity scheduling," *submitted to IEEE Trans. on Inform. Theory*, Dec. 2010. [Online]. Available: http://arxiv.org/abs/1012.3198

[12] J. G. Proakis, *Digital Communications*. McGraw-Hill, 2000.

[13] T. L. Marzetta and B. M. Hochwald, "Capacity of a mobile multiple-antenna communication link in Rayleigh flat fading," *IEEE Trans. on Inform. Theory*, vol. 45, no. 1, pp. 139–157, Jan. 1999.

[14] L. Zheng and D. N. C. Tse, "Communication on the Grassmann manifold: a geometric approach to the noncoherent multiple-antenna channel," *IEEE Trans. on Inform. Theory*, vol. 48, no. 2, pp. 359–383, Feb. 2002.

[15] B. Hassibi and B. M. Hochwald, "How much training is needed in multiple-antenna wireless links?" *IEEE Trans. on Inform. Theory*, vol. 49, no. 4, pp. 951–963, Apr. 2003.

[16] G. Caire, N. Jindal, M. Kobayashi, and N. Ravindran, "Multiuser MIMO achievable rates with downlink training and channel state feedback," *IEEE Trans. on Inform. Theory*, vol. 56, no. 6, pp. 2845–2866, June 2010.

[17] T. L. Marzetta, "How much training is required for multiuser MIMO?" in *Proc. IEEE Asilomar Conf. on Signals, Systems, and Computers (ACSSC)*, Pacific Grove, CA, Oct. 2006.

[18] ——, "Noncooperative cellular wireless with unlimited numbers of base station antennas," *IEEE Trans. on Wireless Commun.*, vol. 9, no. 11, pp. 3590–3600, Nov. 2010.

[19] J. Jose, A. Ashikhmin, T. L. Marzetta, and S. Vishwanath, "Pilot contamination and precoding in multi-cell TDD systems," *accepted for publication in IEEE Trans. on Wireless Commun.*, 2011. [Online]. Available: http://arxiv.org/abs/0901.1703

[20] A. M. Tulino and S. Verdú, *Random Matrix Theory and Wireless Communications*. Foundations and Trends in Communications and Information Theory, 2004, vol. 1, no. 1.

[21] H. Huh, S.-H. Moon, Y.-T. Kim, I. Lee, and G. Caire, "Multi-cell MIMO downlink with cell cooperation and fair scheduling: a large-system limit analysis," *submitted to IEEE Trans. on Inform. Theory*, June 2010. [Online]. Available: http://arxiv.org/abs/1006.2162

[22] A. L. Moustakas, S. H. Simon, and A. M. Sengupta, "MIMO capacity through correlated channels in the presence of correlated interferers and noise: a (not so) large N analysis," *IEEE Trans. on Inform. Theory*, vol. 49, no. 10, pp. 2545–2561, Oct. 2003.

[23] K. R. Kumar, G. Caire, and A. Moustakas, "Asymptotic performance of linear receivers in MIMO fading channels," *IEEE Trans. on Inform. Theory*, vol. 55, no. 10, pp. 4398–4418, Oct. 2009.

[24] A. Forenza, M. Airy, M. Kountouris, R. Heath Jr, D. Gesbert, and S. Shakkottai, "Performance of the MIMO downlink channel with multi-mode adaptation and scheduling," in *IEEE Workshop on Signal Processing Advances in Wireless Communications (SPAWC)*, June 2005, pp. 695–699.

[25] A. Papadogiannis, D. Gesbert, and E. Hardouin, "A dynamic clustering approach in wireless networks with multi-cell cooperative processing," in *Proc. IEEE Int. Conf. on Commun. (ICC)*, May 2008, pp. 4033–4037.

[26] R. Chen, Z. Shen, J. Andrews, and R. Heath, "Multimode transmission for multiuser MIMO systems with block diagonalization," *IEEE Trans. on Sig. Proc.*, vol. 56, no. 7, pp. 3294–3302, July 2008.

[27] H. Shirani-Mehr, G. Caire, and M. J. Neely, "MIMO downlink scheduling with non-perfect channel state knowledge," *IEEE Trans. on Commun.*, vol. 58, no. 7, pp. 2055–2066, July 2010.

[28] H. C. Papadopoulos, G. Caire, and S. A. Ramprashad, "Achieving large spectral efficiencies from MU-MIMO with tens of antennas: location-adaptive TDD MU-MIMO design and user scheduling," in *Proc. IEEE Asilomar Conf. on Signals, Systems, and Computers (ACSSC)*, Pacific Grove, CA, Nov. 2010.

[29] J. Mo and J. Walrand, "Fair end-to-end window-based congestion control," *IEEE/ACM Trans. on Networking*, vol. 8, pp. 556–567, Oct. 2000.

[30] P. Viswanath, D. N. C. Tse, and R. Laroia, "Opportunistic beamforming using dumb antennas," *IEEE Trans. on Inform. Theory*, vol. 48, no. 6, pp. 1277–1294, June 2002.

[31] P. Bender, P. Black, M. Grob, R. Padovani, N. Sindhushayana, and A. Viterbi, "CDMA/HDR: A bandwidth-efficient high-speed wireless data service for nomadic users," *IEEE Commun. Mag.*, vol. 38, no. 7, pp. 70–77, July 2000.

[32] S. Parkvall, E. Englund, M. Lundevall, and J. Torsner, "Evolving 3G mobile systems: Broadband and broadcast services in WCDMA," *IEEE Commun. Mag.*, vol. 44, no. 2, pp. 30–36, Feb. 2006.

[33] D. Aktas, M. N. Bacha, J. S. Evans, and S. V. Hanly, "Scaling results on the sum capacity of cellular networks with MIMO links," *IEEE Trans. on Inform. Theory*, vol. 52, no. 7, pp. 3264–3274, July 2006.

[34] J. Hoydis, M. Kobayashi, and M. Debbah, "On the optimal number of cooperative base stations in network MIMO systems," *submitted to IEEE Trans. on Sig. Proc.*, Mar. 2010. [Online]. Available: http://arxiv.org/abs/1003.0332

[35] R. Zakhour and S. V. Hanly, "Base station cooperation on the downlink: large system analysis," *submitted to IEEE J. Select. Areas Commun.*, June 2010. [Online]. Available: http://arxiv.org/abs/1006.3360

[36] 3GPP technical specification group radio access network, "Further advancements for E-UTRA: physical layer aspects," 3GPP TR 36.814, Tech. Rep., Mar. 2010.

[37] IEEE 802.16 broadband wireless access working group, "IEEE 802.16m evaluation methodology document (EMD)," IEEE 802.16m-08/004, Tech. Rep., Jan. 2009.

[38] T. S. Rappaport, *Wireless Communications: Principles & Practice*. Prentice Hall, 2002.

[39] T. M. Cover and J. A. Thomas, *Elements of Information Theory*. Wiley, 2005.

[40] S. Verdú and S. Shamai (Shitz), "Spectral efficiency of CDMA with random spreading," *IEEE Trans. on Inform. Theory*, vol. 45, no. 2, pp. 622–640, Mar. 1999.

[41] D. N. C. Tse and S. Verdú, "Optimum asymptotic multiuser efficiency of randomly spread CDMA," *IEEE Trans. on Inform. Theory*, vol. 46, no. 6, pp. 2718–2723, Nov. 2000.

[42] C.-N. Chuah, D. N. C. Tse, J. M. Kahn, and R. A. Valenzuela, "Capacity scaling in MIMO wireless systems under correlated fading," *IEEE Trans. on Inform. Theory*, vol. 48, no. 3, pp. 637–650, Mar. 2002.

[43] A. Lozano, A. M. Tulino, and S. Verdú, "Multiple-antenna capacity in the low-power regime," *IEEE Trans. on Inform. Theory*, vol. 49, no. 10, pp. 2527–2544, Oct. 2003.

[44] A. M. Tulino, A. Lozano, and S. Verdú, "Impact of antenna correlation on the capacity of multiantenna channels," *IEEE Trans. on Inform. Theory*, vol. 51, no. 7, pp. 2491–2509, July 2005.

[45] M. Debbah and R. R. Muller, "MIMO channel modeling and the principle of maximum entropy," *IEEE Trans. on Inform. Theory*, vol. 51, no. 5, pp. 1667–1690, May 2005.

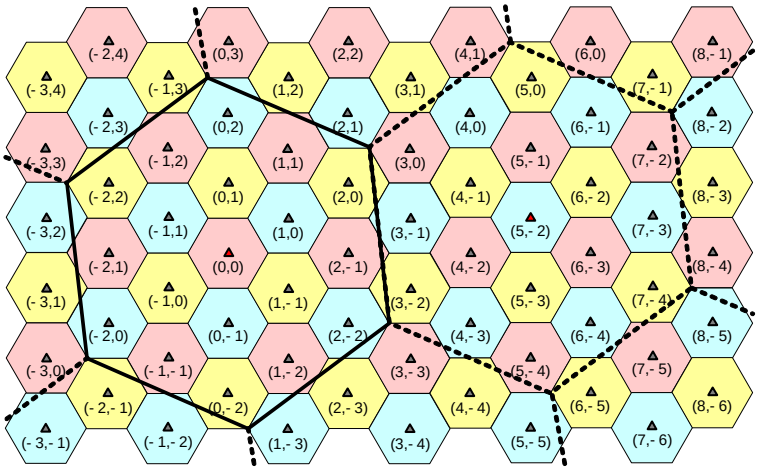

Fig. 1. Two dimensional hexagonal cell layout with $B = 19$. The triangle marks indicate the BS positions (points of $\Lambda_{\rm bs}$) and the red triangle marks indicate the points of Λ. The insides of the large thick-lined hexagon and the small hexagons denote $\mathcal{V}$ and $\mathcal{V}_b$ for $b \in \Lambda_{\rm bs}$, respectively.

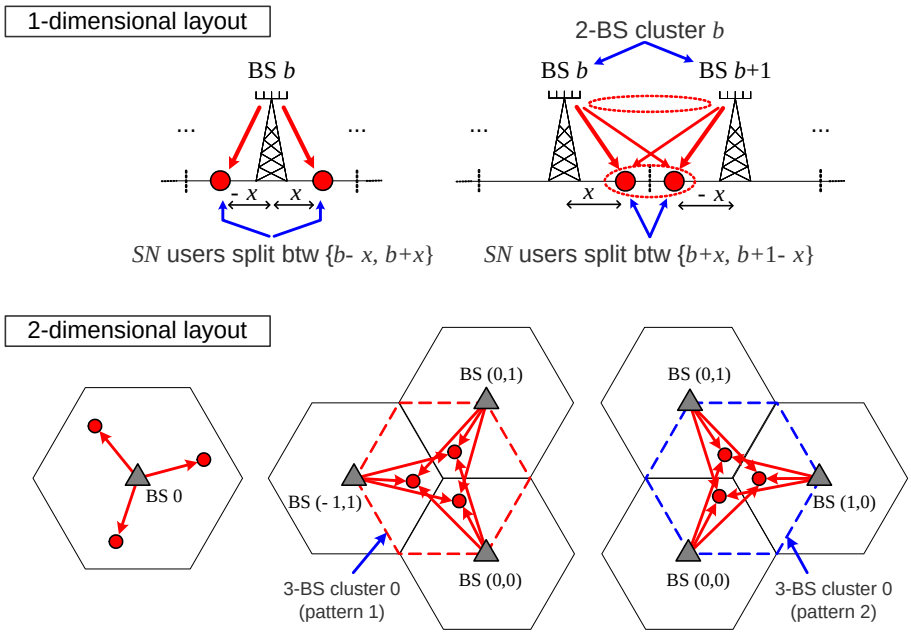

Fig. 2. Cluster pattern geometry and user bins in one-dimensional and two dimensional layouts.

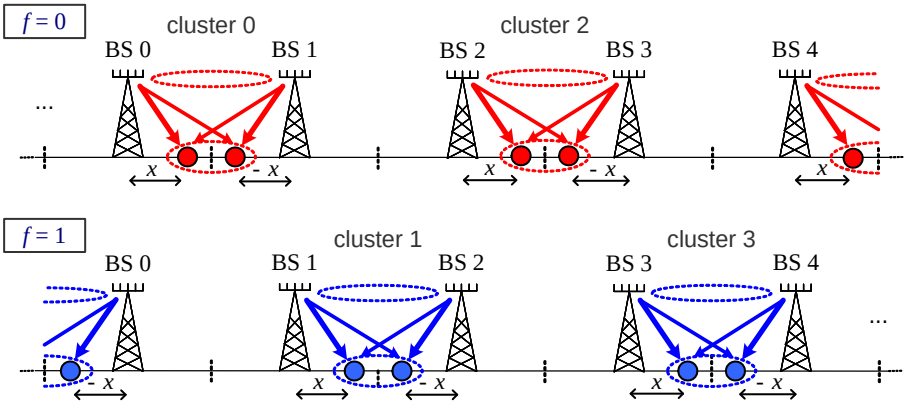

Fig. 3. 1-dimensional layout with $C = 2$ and $F = 2$.

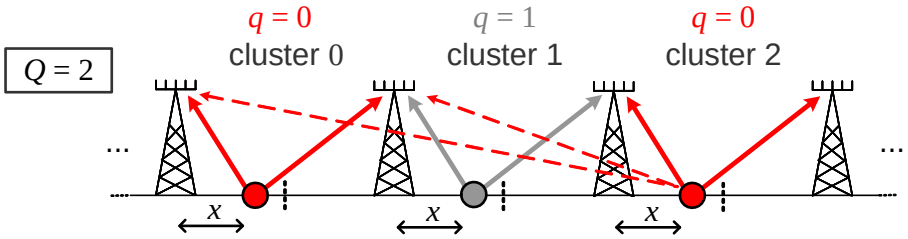

Fig. 4. Pilot reuse and contamination for $C = 2$, $F = 1$, and $Q = 2$. The dashed lines show the contamination from a user sharing the same pilot signal, in another cluster.

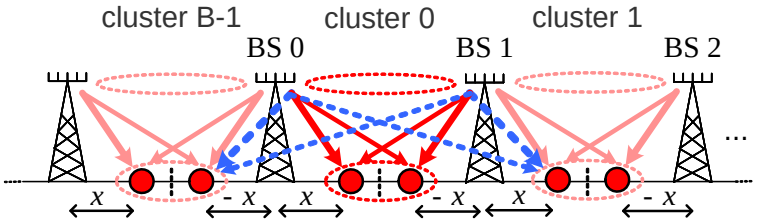

(a) $J = Q$

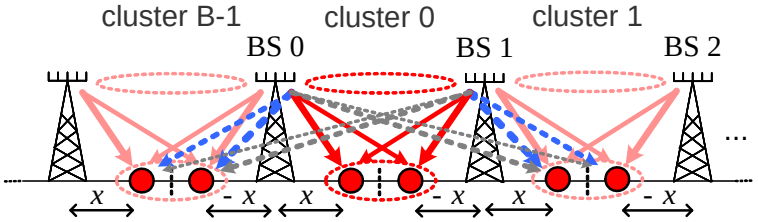

(b) $J = C(Q-1)+1$

Fig. 5. Two cases of a precoding scheme for $C = 2$, $F = 1$, and $Q = 2$, with $J = Q$ (a) and $J = C(Q-1)+1$ (b). The dashed lines indicate the channel vectors to out-of-cluster users for which a ZF constraint is imposed. In Figure (b), the light-shaded dashed lines indicate the channel vectors assumed zero in the beamforming calculation.

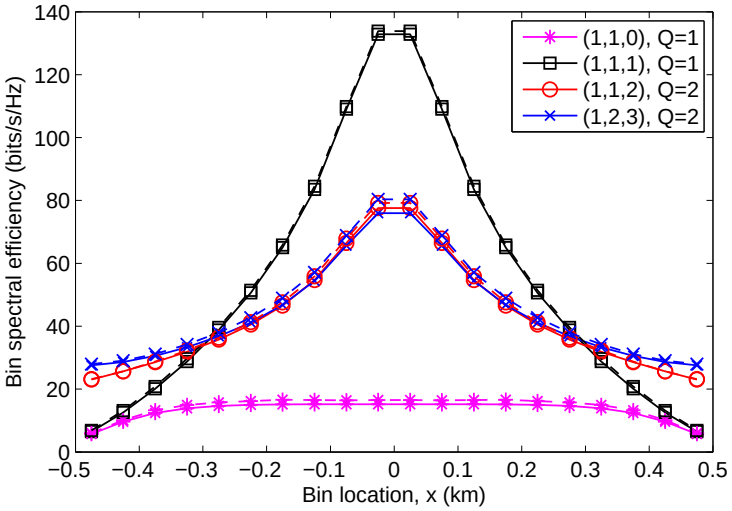

Fig. 6. Bin spectral efficiency vs. location within a cell obtained from the large system analysis (solid) and the finite dimension ($N = 1$) simulation (dotted) for various (F, C, J). $M = 30$ and $L = 40$.

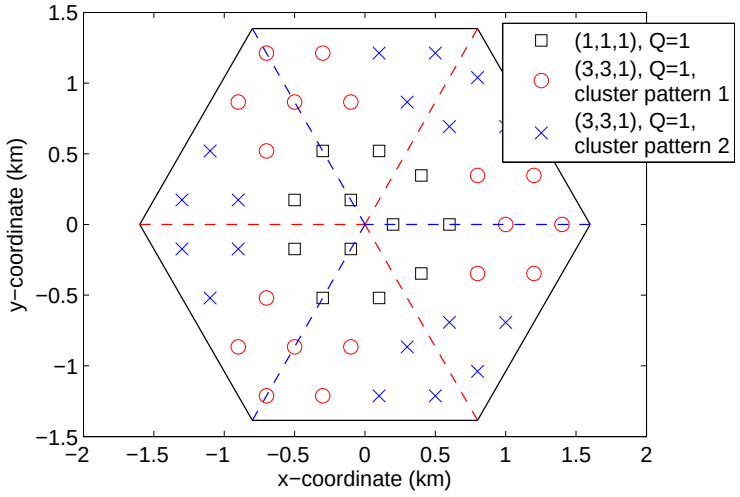

(a) M=20

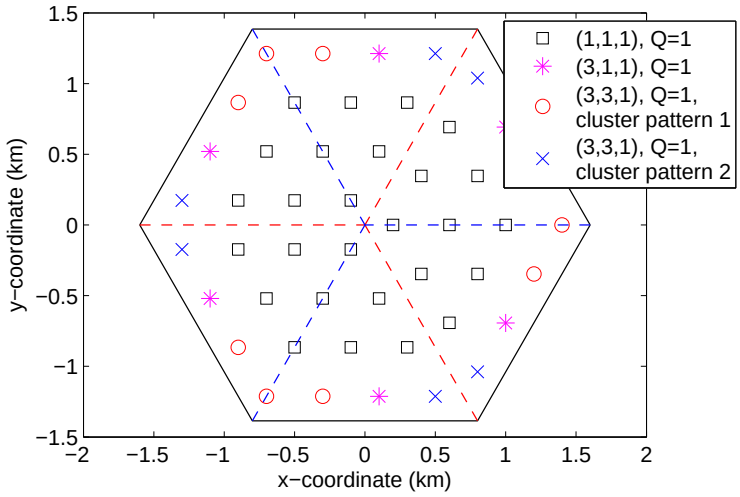

(b) M=100

Fig. 7. Optimal scheme at each user locations. $M = 20$ and 100, $K = 16$, and $L = 84$.

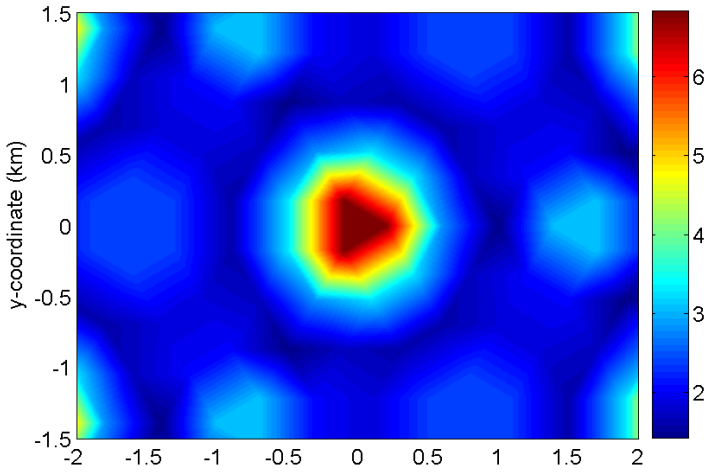

Fig. 8. Bin-optimized spectral efficiencies normalized by the (1,1,0) spectral efficiencies. $M = 50$, $K = 48$,and $L = 84$.

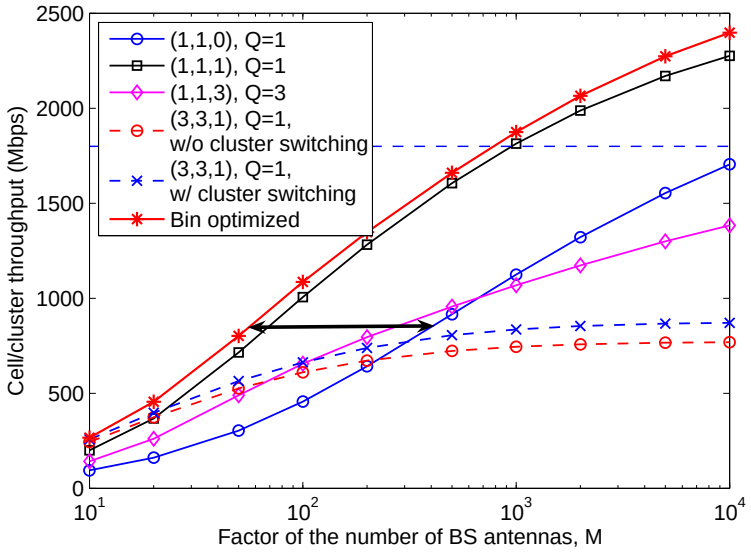

Fig. 9. Cluster sum throughput vs. M for various (F, C, J) and for a bin-optimized architecture under PF scheduling. $K = 48$ and $L = 84$. The arrow indicates that the proposed architecture achieves the same spectral efficiency as the fixed scheme $(1, 1, 0)$ of [18], with a 10-fold reduction of the number of BS antennas.